https://doi.org/10.5194/egusphere-2026-4522
Preprint. Discussion started: 13 August 2026

The MESSy chamber DWARF: a box model for simulating chamber experiments (based on MESSy v2.55.2)

Duong H. Do[1], Astrid Kerkweg[1], Yarê Baker[1,a], Birger Bohn[1], Hendrik Fuchs[1,2], Quanfu He[1,b], Thorsten Hohaus[1], Sungah Kang[1], Timo Kirfel[1], Finja Löher[3,4,c], Niklas Diepenthal[1], Anke C. Nölscher[1,3,4], Anna Novelli[1], Alexander Pschera[1,d], Felix Wieser[1], Sören R. Zorn[1], Andreas Wahner[1], and Domenico Taraborrelli[1]

[1]Institute of Climate and Energy Systems - Troposphere (ICE-3), Forschungszentrum Jülich GmbH, Jülich, Germany
[2]Department of Physics, University of Cologne, Cologne, Germany
[3]Department of Atmospheric Chemistry, University of Bayreuth, Bayreuth, Germany
[4]Bayreuth Center of Ecology and Environmental Research (BayCEER), University of Bayreuth, 95447 Bayreuth, Germany
[a]now at Leibniz Institute for Tropospheric Research (TROPOS), Leipzig, Germany
[b]now at Earth, Ocean, and Atmospheric Sciences Thrust at Hong Kong University of Science and Technology, Guangzhou, China
[c]now at Department of Chemistry, University of York, United Kingdom
[d]now at Faculty of Mathematics and Natural Sciences, University of Cologne, Cologne, Germany

Correspondence: Duong H. Do (h.do@fz-juelich.de) and Domenico Taraborrelli (d.taraborrelli@fz-juelich.de)

Abstract. Numerical simulation of environmental chamber experiments is essential for improving models of atmospheric composition. This task often relies on box models, which are not integral to three-dimensional atmospheric chemical transport models. Here, we present an application of the Modular Earth Submodel System (MESSy) DWARF model for chamber simulation experiments. It was developed as a zero-dimensional chemical box model of atmospheric oxidation. Chamber-specific features—including the injection of trace gases, variable radiation conditions, gas- and aqueous-phase chemistry, wall emissions, and dilution—are represented using existing and adapted MESSy submodels. We describe the multi-phase kinetic framework, the estimation of aerosol liquid water content and a simplified treatment of wall losses. We tested the MESSy chamber DWARF setup with experiments from three environmental chambers: The SAPHIR and SAPHIR-STAR chambers at Forschungszentrum Jülich, and the BATCH chamber at the University of Bayreuth. These chambers cover diverse designs and experimental conditions. The model reproduces observed time series of radicals, nitrogen oxides and ozone during an experiment in SAPHIR in which 2-methyl-3-butene-2-ol was oxidised. In another test the model was used to check the consistency of the experimental boundary conditions in the BATCH chamber. Further chamber DWARF tests also show that the framework can predict organic aerosol mass concentration via kinetic partitioning between the gas phase and deliquescent particles in SAPHIR-STAR. Modeled organic mass concentration during this experiment where α-pinene was oxidised agrees well with observations, supporting the framework's ability to simulate the chemical evolution in both the gaseous and aqueous phase. The MESSy chamber DWARF provides a useful tool for developing and

https://doi.org/10.5194/egusphere-2026-4522
Preprint. Discussion started: 13 August 2026

evaluating kinetic models. Within this framework, we can test new laboratory findings directly for their atmospheric relevance. Thanks to the MESSy framework, we can use the same kinetic model for global simulations.

1 Introduction

Understanding the processes in atmospheric chemistry is key to predicting and mitigating the effects of air pollution and climate change. Combining laboratory experiments and modeling is therefore crucial for advancing knowledge in this field. Laboratory studies conducted in controlled environmental chambers enable in-depth investigations of specific chemical mechanisms or physical processes that are relevant in the atmosphere (Fuchs et al., 2026). However, it is challenging to assess the atmospheric impact of findings from chamber experiments at global scale. In fact, global chemical-transport models often include very simplified schemes for chemistry and aerosol microphysics. It is therefore desirable to have an atmospheric model that can be used for simulating both, chamber experiments and the global atmosphere. This model must operate at the same level of detail with respect to the chemical kinetic model.

Existing zero-dimensional chemical box models demonstrate the ability to simulate chamber experiments and test chemical mechanisms. These models provide a detailed understanding of chemical kinetics and some also of aerosol microphysics. The aim of these models is to evaluate and improve chemical mechanisms. If used to simulate chamber experiments, they often also include the description of injections, dilution, artificial illumination and exchanges with the chamber wall. However, these models are typically not components of three-dimensional models. Such models are designed for a broader user base by utilizing user-friendly programming languages. This is the case for models like EASY (Karl, 2004), PyCHAM (O'Meara et al., 2021) and F0AM (Wolfe et al., 2016). Other models like AtChem (Sommariva et al., 2020) provide an interactive user interface. Global atmospheric models are on the other hand written in Fortran and setup to work with highly reduced chemical mechanisms. Thus the knowledge transfer from chamber experiments to global models is not trivial and inherently bears limitations when going from a detailed to a lumped kinetic model. Another chemical box model that has been developed originally as part of the MESSy (Modular Earth Submodel System) modeling framework is CAABA/MECCA (Sander et al., 2011). However, CAABA/MECCA offers only a subset of the many functionalities available within the MESSy framework. All these box models are restricted to a zero-dimensional framework with no seamless way to represent their detailed process representations in three-dimensional simulations.

Instead of being a stand-alone chemical box model, the MESSy DWARF model (Kerkweg et al., 2025) is an integral part of the MESSy framework (Jöckel et al., 2005). MESSy DWARF acts as a very simplistic model driver compared to the frequently used dynamical three-dimensional base models, e.g., ECHAM5 (Roeckner et al., 2006;

https://doi.org/10.5194/egusphere-2026-4522
Preprint. Discussion started: 13 August 2026

Jöckel et al., 2010) or COnsortium for Small-scale MOdeling (COSMO) (Rockel et al., 2008; Kerkweg and Jöckel, 2012). The process descriptions, implemented in the respective MESSy submodels, can be refined and used for both the zero-dimensional and three-dimensional simulations without any further adaptation. MESSy is a well-established modeling framework for Earth System Modeling (ESM) that has been utilized in numerous studies and publications (Jöckel et al., 2010, 2016). While the primary focus of MESSy is on chemistry-climate and air quality applications in three-dimensional model grids, the recently developed MESSy DWARF allows to perform zero-dimensional simulations based on the MESSy framework. This box model is capable of utilizing all MESSy capabilities. It allows the representation of chemical and physical processes in chamber experiments based on existing MESSy submodels. For instance, gas- and aqueous-phase reactions, phase partitioning, dilution, injections of trace gases, or losses of gaseous species to the chamber wall can be described by MESSy submodels. The framework allows for the transfer of new findings from the chamber experiment to the global scale.

The DWARF configuration used in this study is referred to as "chamber DWARF". The chamber DWARF is tested by comparing the model predictions to observations of experiments in three chambers with different properties (Tab. 1). The chambers are:

1. The "Simulation of Atmospheric PHotochemistry In a large Reaction chamber" (SAPHIR) chamber is an outdoor atmospheric simulation chamber at Forschungszentrum Jülich, Germany (Bohn and Zilken, 2005).
2. The SAPHIR "STirred Atmospheric flow Reactor" (STAR) chamber, also located at Forschungszentrum Jülich, is an indoor continuously stirred glass tank chamber (Baker et al., 2024).
3. The "Bayreuth ATmospheric simulation CHamber" (BATCH) Teflon chamber described by Löher et al. (2024) is an indoor chamber.

Table 1: Specification of main chamber characteristics.

Property	SAPHIR	SAPHIR-STAR	BATCH
Wall material	Teflon	Glass	Teflon
Volume (m^3)	270	2	0.3
Operating mode	Batch	Steady-State	Batch
Dilution	Yes	No	No
Light	Sunlight	Artificial (UV)	Artificial (UV-Vis)

The aim of this article is to describe the developments and the methodology for conducting zero-dimensional multi-phase kinetics simulations of chamber experiments.

https://doi.org/10.5194/egusphere-2026-4522
Preprint. Discussion started: 13 August 2026

2 Model description

2.1 The MESSy DWARF

The DWARF base model as part of the MESSy framework is used to construct a zero-dimensional, multi-phase chemistry box model. The most important property of MESSy in this context is its modular structure. Each process type is represented by an individual so-called submodel. This usually comprises of two software layers: (i) a core layer which is independent of the base model and contains the implementation of the respective process in its basic entity (i.e., mostly for a box or column), and (ii) the submodel interface layer which handles the data exchange between the core layer and the overarching MESSy infrastructure (for more details see Kerkweg et al., 2025). MESSy's modular design offers users the flexibility to customize the configuration to their research objectives.

In MESSy and thus in the chamber DWARF, the configurations of the simulation are mainly controlled via Fortran90 namelists (Jöckel et al., 2005; Kerkweg et al., 2025). Each MESSy submodel is associated with a namelist file, which in turn contains one or more Fortran90 namelists. The `&CRTL` namelist controls the physical core, e.g., switches between specific parametrisations or scaling factors which can be specified. The `&CPL` namelist controls the coupling of the respective submodel to the MESSy infrastructure and thus to the other MESSy submodels. The chamber DWARF configuration contains a subset of the MESSy submodels, which are suitable for modeling chamber experiments. Section 4 provides an overview of how selected submodels are utilized to reproduce specific processes of chamber experiments.

2.2 Workflow

This section provides a comprehensive overview of the chamber DWARF's workflow for simulating chamber experiments. Figure 1 illustrates the standard workflow for a chamber DWARF simulation. For each chamber experiment, the input data are pre-processed to ensure its compatibility with the model. In addition, the user can customise the automatically generated name lists and the chemical mechanism, including the number of aqueous phases considered in the simulation.

The Fortran90 namelists of the individual submodels used for the simulation of chamber experiments are mostly created via scripts. However, the user can edit them to adapt the model to the respective experiment, e.g., to refine an injection or the dilution rate. The model needs to be compiled once to run the simulation. Re-compilation is only required if the model source code is modified, for example by changing the chemical mechanism. Depending on whether the chamber experiments are carried out with aerosol seeding or manifest nucleation, the number of aerosol phases need to be chosen accordingly. Furthermore, the exchange of trace gases with the chamber wall can be taken into account.

A Python script was developed to facilitate the users' data processing. This script is capable of automatically generating a model input data package, including the pre-processed data in a single folder and the required control namelist in a separate folder. The processed measurement data can then be read as input of the model and thus be

https://doi.org/10.5194/egusphere-2026-4522
Preprint. Discussion started: 13 August 2026

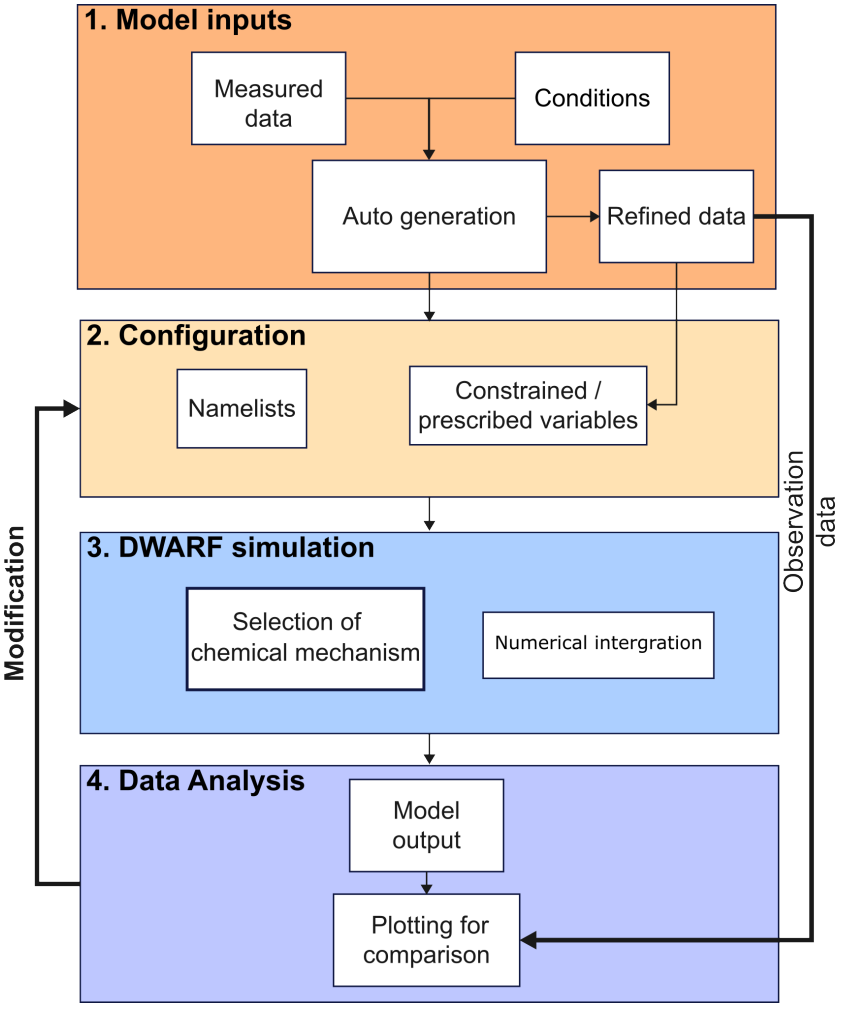

Figure 1. Workflow of a chamber DWARF simulation. Step 1: Input data is processed by converting measured data to a format readable by the model via auto generation scripts. 2. Create a model configuration via the scripts, optionally refined namelists and by setting constrained/prescribed variables. 3. Simulation. 4. Plotting model output versus observation data. The cycle can be repeated, if modifications are required until model-measurement agreement is obtained.

https://doi.org/10.5194/egusphere-2026-4522
Preprint. Discussion started: 13 August 2026

used for constraining a variable during the simulation and, additionally, can be plotted afterwards to be compared with the model results. The edited control namelist is created according to the simulation's requirements, including constrained variables and the application of dilution rate constants. By providing the file path to the data of one chamber experiment, the build-in Python script creates another folder to store the pre-processed data with the associated chamber's name and experiment date. The directory of pre-processed data is then used by the model to read the processed observational data for the simulation.

3 Prescribed and constrained variables

The chamber DWARF offers two options for constraining the simulation to observations. First, all data required to constrain the simulation must be read by the model. These data are then either assigned directly to the respective variable, which is not changed by any other processes, i.e. it remains constant, or the variable is initialized to the observed value at every time step. The value of the latter can change between two time steps due to the modeled chemical and physical processes.

3.1 Physical parameters

Typically, physical parameters including temperature, (relative) humidity, pressure, and dilution rates are constrained in the model to measurements. These parameters are essential, as they are, e.g., important for calculating chemical reaction rates and the gas-particle phase partitioning. They are kept constant at the observed value during the integration.

3.2 Chemical species

In the context of a particular chemical mechanism, closed-shell molecules or radicals are referred to as chemical species or tracers. Users can freely select, which tracers are constrained in a specific model simulation.

For constraining it, the concentration of a chemical species is initialized to an observed value for each time step (Sect. 4.2.2) and can be changed in between due to chemical and physical processes. However, a species can optionally be declared as 'fixed' for the numerical integrator. In this way, the concentration of the respective species does not change while the chemical ordinary differential equation (ODE) system is being solved. This prevents the species from changing as a result of chemical processes. If the species is also excluded from all physical processes (such as dilution), the species remains constant during the time step, i.e. until a new observed value is assigned.

The concentrations of O_2 and N_2 are essential for defining the conditions in the chamber. They are initialized with either measurements or set to constant values.

https://doi.org/10.5194/egusphere-2026-4522
Preprint. Discussion started: 13 August 2026

3.3 Photolysis frequencies

In the chamber DWARF, the photolysis frequencies (J) required for the photochemical reactions are constrained to values derived from measurements. The three chambers considered in this study use different types of light sources: one natural sunlight and two artificial lamps (Tab. 1).

For the SAPHIR chamber, photolysis frequencies J_{exp} are calculated for each experiment based on measured actinic flux densities (Bohn and Zilken, 2005; Bohn et al., 2005). If a photolysis frequency for a species i is not available in the dataset of the experiment, it is estimated by scaling the photolysis frequency J_{MCM} calculated from the parameterization provided by the Master Chemical Mechanism (MCM) for clear-sky conditions (Jenkin et al., 1997) using the current solar zenith angle. A scaling factor (F_{scal}) is applied to account for the difference between calculated and measured J-values, for example due to the transmission of the Teflon film or clouds:

$$J_{exp}(i) = F_{scal} \cdot J_{MCM}(i) \tag{1}$$

The scaling factor for a species i is determined by Eq. (2) as outlined in Fuchs et al. (2013) and Sommariva et al. (2020):

$$F_{scal} = \frac{J_{exp}(NO_2)}{J_{MCM}(NO_2)} \tag{2}$$

where J_{exp} and J_{MCM} are the experimentally determined and parameterized NO_2 photolysis frequencies.

The SAPHIR-STAR and BATCH chambers use artificial light sources providing stable radiation conditions during an experiment. For SAPHIR-STAR experiments, UV-C and UV-A lamps are used to photolyze O_3 and NO_2. Their respective J-values were determined in reference experiments from the photo-chemical equilibrium between O_3, NO and NO_2. For BATCH experiments, the J-values were calculated using the measured spectral irradiance of the solar simulator, recommended absorption cross sections and quantum yields in the spectral range $\lambda = 262 - 1000$ nm (Löher et al., 2024). A summary of the J-values used for each chamber experiment in this work is given in Tab. 2.

Table 2: Photolysis frequencies (J) typical for the three chambers. J(O^1D) is the photolysis frequency for the reaction $O_3 + h\nu \rightarrow O(^1D)$. J($NO_2$) is the photolysis frequency for the reaction $NO_2 + h\nu \rightarrow NO + O(^3P)$.

Chamber	J(O^1D) / s^{-1}	J(NO_2) / s^{-1}	other J
SAPHIR	0.2-1.5 10^{-5}	3-5 10^{-3}	calculated or scaled
SAPHIR-STAR	1.2-1.5 10^{-3}	$\approx$ 1.2 10^{-3}	-
BATCH	$\approx$ 7.5 10^{-5}	$\approx$ 2.1 10^{-2}	calculated

3.4 Aerosol properties

The aerosol mean radius of number size distribution and number concentration are required for the calculation of the aerosol liquid water content ($ALWC$). The latter affects the partitioning of chemical species between gas and

https://doi.org/10.5194/egusphere-2026-4522
Preprint. Discussion started: 13 August 2026

aerosol phase in the chamber DWARF. In experiments with particles, number size distributions are typically analyzed using a scanning mobility particle sizer (SMPS) instrument. Measurements are then used by chamber DWARF. The total number concentration of particles, the standard deviation of the log-normal distribution (σ), and the mean diameter determined from the number size distribution are prescribed and used to estimate the volume of the wet particles in the model. Henceforth, the terms "wet particle volume" and "wet radius" will be used to refer to the particle properties derived from SMPS measurements in this work. In addition, the observation of the inorganic particle mass is used to estimate the dry particle volume (or volume of solutes in the aerosol phase). The inorganic composition is either constrained to observations by instruments, such as an aerosol mass spectrometer (AMS) and an ion chromatography (IC), or calculated using information about the amount of injected material.

4 Model representation of chamber processes

In the MESSy modeling system, individual atmospheric processes are implemented as independent submodels. This section presents the submodels used in the chamber DWARF. Each submodel is controlled via a configuration file (Sect. S1. provides the details of the respective settings). Figure 2 presents an overview of the submodels simulating the associated processes. The submodel IMPORT is used to import data from external files. It reads the observational data required to constrain the simulation to the respective experimental conditions. The SCALC submodel enables the execution of mathematical operations on data for each simulation time step. The TREXP submodel simulates the dilution process and it can be used to simulate continuous injections of trace gases. The PTRACINI submodel is used for simulating the instantaneous injections of trace gases and for constraining the mixing ratios of chemical species. Finally, the MECCA submodel solves multi-phase chemical kinetics including phase partitioning (Sect. 5). Illustrative examples of the respective submodel namelist files are provided and explained further in the supplement (Sect. S1.).

4.1 Dilution of trace gases

In a chamber experiment, the continuous flow of air affects the species concentrations in different ways. A constant flow of synthetic air can serve to maintain the pressure in the chamber, thereby for example preventing the diffusion of ambient air into the chamber. In the SAPHIR chamber, the replenishment flow dilutes the chemical concentrations with a typical rate constant of 1.4×10^{-5} s^{-1}, which leads to a dilution of 5 % per hour. In the SAPHIR-STAR chamber, the typical flow results in a residence time of 63 minutes, equivalent to a loss rate constant of 2.5×10^{-4} s^{-1} for all species.

For simulating the dilution of a chemical species in a chamber, the submodel TREXP (Tracer Release EXperiments from Point sources) is applied. The actual decay rate is calculated in each simulation by dividing the measured chamber flow rate by the chamber volume.

https://doi.org/10.5194/egusphere-2026-4522
Preprint. Discussion started: 13 August 2026

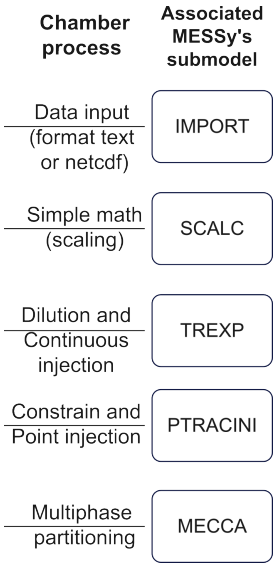

Figure 2. MESSy submodels for simulating chamber experiment.

4.2 Injection of trace gases

The injection of precursors is a fundamental process when conducting chamber experiments. Two types of injection are implemented in the chamber DWARF: injections at a specific point in time (point-in-time injection) and continuous injections.

4.2.1 Point-in-time injections

The point-in-time injection is a process, when a defined quantity of a trace gas is introduced into the environmental chamber at a certain point in time. This can be achieved by rapidly evaporating a liquid species while injecting it using a syringe or by a fast addition of a gas-phase species using a mass flow controller. If the mixing time is negligible, the mixing ratio of the injected compound can be set to the expected or measured value at the model time step. In the model, point-in-time injections are implemented using the PTRACINI submodel (Kerkweg et al., 2025). In the PTRACINI namelist, the concentration of a specific species can be set to a fixed value at a specified point in time (Kerkweg et al., 2025, Appendix A). Figure S1 illustrates an example of the syntax for simulating a point-in-time injection.

https://doi.org/10.5194/egusphere-2026-4522
Preprint. Discussion started: 13 August 2026

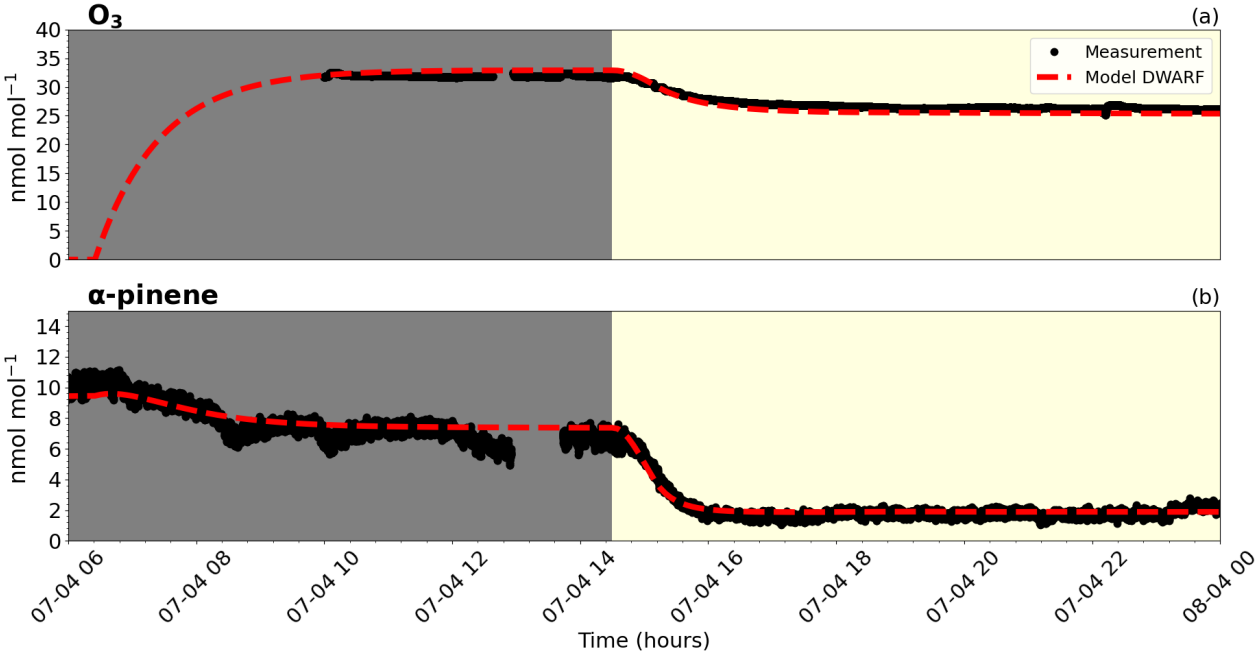

Figure 3. Modeled and measured ozone and α-pinene concentrations during an experiment in SAPHIR-STAR. α-pinene was injected at a rate of 260 nL/h resulting in a steady-state concentration of 10 nmol/mol in the chamber. The first phase, where only α-pinene was injected and concentrations reached steady-state conditions, is not shown. The simulation time starts with the injection of ozone into the system. The ozone concentration was slightly above the target concentration of 30 nmol/mol. Eight hours after the beginning of the experiments the photooxidation phase was started by turning on the UV-C (254 nm) lights, indicated by the change of the background from gray to yellow. In the dark, the concentration of ozone increases with the time constant of the air exchange rate and reaches steady-state concentrations determined by the constant injection rate and the loss from ozonolysis of α-pinene, which concentration is accordingly decreasing. When the lights (UV-C) are turned on, α-pinene is additionally lost by the reaction with OH, which is photochemically formed from ozone photolysis, leading to a decrease of the ozone concentration. During certain periods, instruments were switched to measure the inflow concentrations lines therefore the measured data was unavailable.

4.2.2 Continuous injections

During a continuous injection a chemical species is introduced into a chamber at a constant rate over a specified period of time. For example, in an experiment conducted in steady-state mode, chemicals are introduced at a
205 constant rate throughout the experiments. The MESSy submodel TREXP (Jöckel et al., 2010) is used to simulate this continuous injection. The injection rate, start time, and end time can be adjusted via the namelist file of the TREXP submodel (Fig. S2).

https://doi.org/10.5194/egusphere-2026-4522
Preprint. Discussion started: 13 August 2026

To validate the model performance, a simulation was conducted to reproduce an experiment in which α-pinene and O_3 were continuously injected in the SAPHIR-STAR chamber. In this experiment, the injections of ozone and α-pinene started in the dark, when no photolysis reactions occurred in the chamber. Thus, only ozonolysis of α-pinene was taking place. The initial injection rate of O_3 and α-pinene in chamber DWARF is adjusted to match their measured concentration in the dark phase, then remains constant to the end of the simulation. Subsequently, the chamber lights were switched on to establish photo-chemical reactions. The model successfully reproduces the decrease of both O_3 and α-pinene to the observed mixing ratios.

Figure 3 shows the comparison between model simulation and measurements. During steady-state conditions in the dark phase, the measured concentrations stabilized at approximately $32\,\mathrm{nmol\,mol^{-1}}$ for ozone and $7\,\mathrm{nmol\,mol^{-1}}$ for α-pinene. The photochemical regime was established when the light was switched on, leading to increased losses of O_3 by photolysis, and of α-pinene by reaction with OH. The initial injection rate of O_3 and α-pinene in chamber DWARF is adjusted to match their measured concentration in the dark phase, then remains constant to the end of the simulation. The time behaviour of the transition of the O_3 concentration to a new steady-state value agrees well between measurements and model results. This example shows that the model is able to well describe the inflow and outflow of steady-state chambers.

5 Multi-phase kinetic framework

The core of the chamber DWARF is the submodel MECCA (Module Efficiently Calculating the Chemistry of the Atmosphere). It implements an atmospheric chemistry model incorporating a comprehensive chemical mechanism encompassing tropospheric and stratospheric chemistry of both the gas and aqueous phases as described in Sander et al. (2019). The gas-phase chemistry is represented by the Mainz Organic Mechanism (MOM) (MOM, Sander et al., 2019), which includes organics up to C_{10}-compounds such as isoprene (Nölscher et al., 2014; Novelli et al., 2020; Taraborrelli et al., 2012), monoterpenes (Mallik et al., 2018; Hens et al., 2014), and aromatics (Cabrera-Perez et al., 2016; Taraborrelli et al., 2021).

Aqueous-phase chemistry of organics up to C_4-compounds is represented by the Jülich Aqueous-phase Mechanism of Organic Chemistry (Rosanka et al., 2021, JAMOC) with updates for formaldehyde chemistry (Franco et al., 2021). Furthermore, the recent developments by Wieser et al. (2024) are taken into account. They include 1) updates for the isoprene + NO_3 and benzene + OH chemistry, 2) a state-of-the-art limonene oxidation scheme and 3) the reactive uptake of epoxydiols yielding tetrols and organosulfates.

Further model developments are implemented in MECCA in this work. Here, we introduce the kinetic partitioning framework for simulating chamber experiments. With the addition of an aerosol phase and a third phase, representing the chamber wall, the kinetic framework is capable of simulating the partitioning processes of various gases within a chamber DWARF setting. The exchange coefficients between the gas and aqueous phases are based on the liquid water content and water solubility as determined by the Henry's law coefficient. Additionally, the loss rate of each

https://doi.org/10.5194/egusphere-2026-4522
Preprint. Discussion started: 13 August 2026

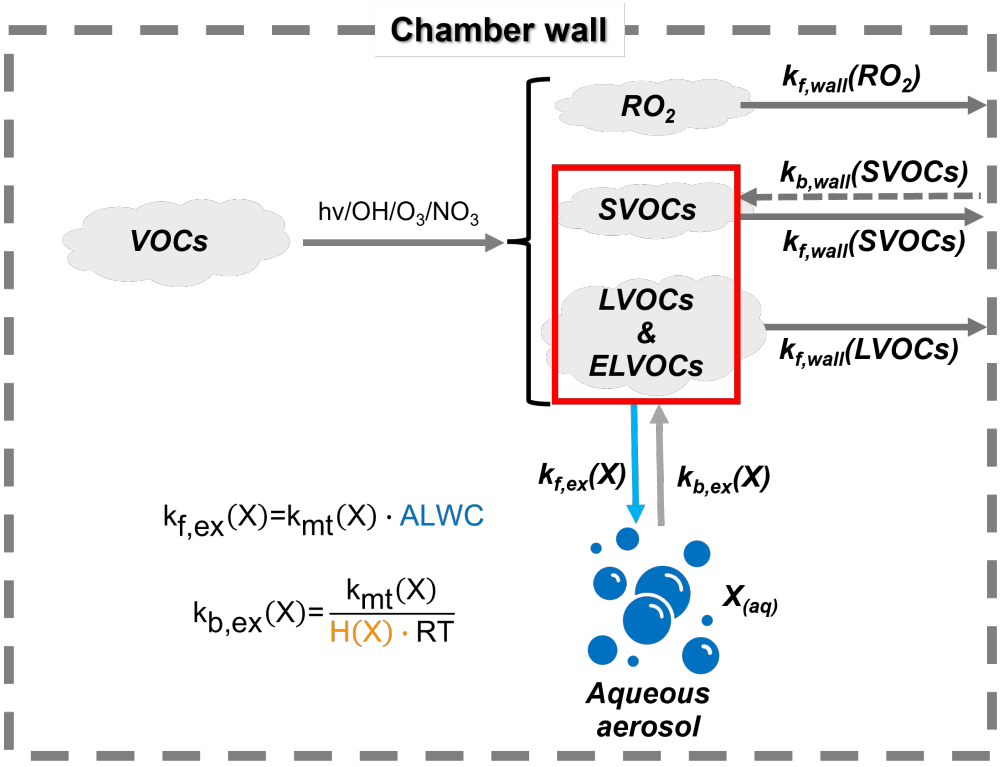

Figure 4. Multi-phase chemistry modeling scheme: water-soluble gases dissolve in aqueous aerosol with the forward exchange rate coefficient ($k_{f,ex}(X)$) whose value depends on the liquid water content ($ALWC$) and the mass transfer coefficient $k_{mt}(X)$. Dissolved organics evaporate to the gas phase by the backward exchange coefficient ($k_{b,ex}(X)$) whose value depends on $k_{mt}(X)$ and the inverse of the Henry's law coefficient $H(X)$. $k_{mt}(X)$ is formulated as defined in Sander (1999). Organic species are classified into volatility groups, with each group characterised by a specific exchange coefficient. RO_2 radicals are treated as an independent group. The coefficients describe the exchange of species between the gas phase and the chamber wall: the forward coefficient ($k_{f,wall}(X)$) is for the uptake of gas-phase species by the chamber wall, and the backward coefficient ($k_{b,wall}(X)$) is for outgassing from the chamber wall.

gas species to the chamber wall can be adjusted for an experiment. The subsequent sections provide a detailed description of the methodology used for the partitioning of the gas species to the aerosol and wall phases.

5.1 Gas-particle phase partitioning

In the three-dimensional model, the partitioning between gas and aqueous phases is usually simulated using independent MESSy submodels describing scavenging (SCAV, Tost et al. (2006)) and/or aerosol partitioning (GMXe-AERCHEM, Rosanka et al. (2024)). However, the MECCA submodel can simulate partitioning across multiple phases with one system of ordinary differential equations. Building on MECCA_AERO (Kerkweg et al., 2007),

https://doi.org/10.5194/egusphere-2026-4522
Preprint. Discussion started: 13 August 2026

the sub-submodel, MECCA_CHAMEXP, was developed for simulating multi-phase chamber experiments with the MESSy DWARF.

Figure 4 illustrates the partitioning scheme implemented in MECCA_CHAMEXP. Adapting the kinetic framework of MECCA_AERO to MECCA_CHAMEXP, the model considers the phase partitioning to be dependent on the water solubility described by Henry's law coefficient of a compound X (H_s^{cp}(X)) and the $ALWC$. The $ALWC$ is a crucial variable and the actual value is calculated differently in simulations for chamber experiments and the global troposphere. At microscopic level, the mass flux across the gas-liquid interface is governed by the kinetic mass transfer coefficient (k_{mt}). This is calculated according to the formulation by Sander (1999) based on the work by Schwartz (1986). The calculation of k_{mt} includes a gas-diffusion term (k_{dg}) and an interfacial mass transport term (k_i). The mass transfer coefficient for the species X is calculated for a single particle as:

$$k_{mt}(X) = \left(\frac{1}{k_{dg}} + \frac{1}{k_i}\right)^{-1} = \left(\frac{r^2}{3D_g(X)} + \frac{4r}{3\overline{v_X}\alpha(X)}\right)^{-1} \tag{3}$$

where, k_{mt} is the mass transfer coefficient ($\mathrm{m^3_{air}\,m^3_{aq}\,s^{-1}}$), r is the particle radius (m), D_g(X) the gas-phase diffusion ($\mathrm{m^2\,s^{-1}}$), α(X) the accommodation coefficient of the given species, and $\overline{v}_X$ ($\mathrm{m\,s^{-1}}$) the mean molecular velocity from the Boltzmann velocity distribution. Then, the forward $k_{f,ex}$(X) and the backward $k_{b,ex}$(X) ($\mathrm{s^{-1}}$) phase-transfer coefficients are calculated at macroscopic level as follow:

$$k_{f,ex}(X) = k_{mt}(X) \cdot LWC \tag{4}$$

$$k_{b,ex}(X) = \frac{k_{mt}(X)}{H_s^{cp}(X) \cdot RT} \tag{5}$$

where the $ALWC$ is the liquid water content ($\mathrm{m^3(aq)\,m^{-3}(air)}$), H_s^{cp} is the Henry's law coefficient ($\mathrm{mol\,m^{-3}\,Pa^{-1}}$), T is the air temperature (K), and R is the universal gas constant ($\mathrm{J\,mol^{-1}\,K^{-1}}$). The Henry's law coefficient of all organic species with respect to water as solvent is estimated by the structure-activity relationship GROMHE (Raventos-Duran et al., 2010). In addition, the temperature-dependence is taken from Wieser et al. (2024).

5.1.1 Aerosol liquid water content

In global simulations, the aerosol submodels (MADE3, GMXe) calculate the aerosol $ALWC$ based on the aerosol properties provided by these submodels. The calculation requires aerosol properties such as the radius of the dry particle (`dry radius`), the radius of the water-containing particle (`wet radius`), and the standard deviation of the log-normal distribution (σ) of the particle size distribution. The model estimates the $ALWC$ by subtracting the volume of the dry particle from that of the wet particle (Eq. 6) where V_{wet} and V_{dry} ($\mathrm{m^3(aq)\,m^{-3}(air)}$) are the volume concentrations of the wet and dry particle, respectively.

$$ALWC = V_{wet} - V_{dry} \tag{6}$$

https://doi.org/10.5194/egusphere-2026-4522
Preprint. Discussion started: 13 August 2026

In chamber DWARF, the volume of the wet particle is estimated by Eq. 7, in which the geometric mean radius of the wet particle size distribution r_{wet} (m), the particle number concentration N ($\#\,\mathrm{cm}^{-3}$) and the geometric standard deviation of the log-normal distribution σ are constrained to measured values by the SMPS instrument. This approach works for direct measurement of particle from chamber by SMPS without drying process.

$$V_{wet} = \frac{4}{3}\pi \cdot r_{wet}^3 \cdot N \cdot \exp\left(\frac{9 \cdot (\log\sigma)^2}{2 \cdot (\log e)^2}\right) \tag{7}$$

The dry particle volume can be calculated using two different methods. The optimal method for the respective problem can be selected in the MECCA control namelist. The first method determines the dry volume V_{dry} as the sum of the inorganic (V_{inorg}) and the organic (V_{org}) volume concentrations of the particles (Eq. 8). V_{inorg} is the total volume of inorganic ions ($\mathrm{SO_4^{2-}}$,$\mathrm{HSO_4^-}$,$\mathrm{NO_3^-}$,$\mathrm{NH_4^+}$) in the particle phase (Eq. 9). V_{org} refers to the total volume of organic species found in the particle phase (Eq. 10). The volume for each species is calculated based on its mass concentration (m) and density (ρ). This method can be used if the inorganic mass concentration is measured.

$$V_{dry} = V_{inorg} + V_{org} \tag{8}$$

$$V_{inorg} = \sum \frac{m_{inorg[i]}}{\rho_{inorg[i]}} \tag{9}$$

$$V_{org} = \sum \frac{m_{org[i]}}{\rho_{org[i]}} \tag{10}$$

The second method uses the particle size growth factor (GF) to estimate the dry particle radius. Under the assumption that the coagulation rate stays constant, the particle growth is primarily due to water uptake. This method employs fitting parameters for estimating the hygroscopic growth of particles at a temperature of 298 K. Therefore, this method is limited to experiments at around 298 K. For other experimental conditions, the volume of the dry matter can be estimated by Eq. 11

$$V_{dry} = \frac{4}{3}\pi \cdot r_{dry}^3 \cdot N \cdot \exp\left(\frac{9 \cdot (\log\sigma)^2}{2 \cdot (\log e)^2}\right) \tag{11}$$

$$r_{dry} = \frac{r_{wet}}{GF_{mix}} \tag{12}$$

$$GF_{mix} = \sqrt[3]{\sum (\varepsilon_i \cdot GF_i^3)} \tag{13}$$

where r_{dry} (m) is the geometric mean radius of particle size distribution for the non-water component in the aqueous phase. The GF_{mix} is the hygroscopic growth factor of particles, which consist of a mixture of inorganic and organic compounds. The Zdanovskii–Stokes–Robinson (ZSR) relation (Stokes and Robinson, 1966) is used to predict the hygroscopic growth factor of the mixed aerosol particle (GF_{mix}) using the growth factor of the pure components `i` (GF_i) and their respective volume fractions, ε_i, in the mixture (Malm and Kreidenweis, 1997; Wang et al., 2021). The growth factor of inorganic and organic compounds can be individually set in the namelist of the MECCA submodel (Sect. S1.4.).

https://doi.org/10.5194/egusphere-2026-4522
Preprint. Discussion started: 13 August 2026

5.1.2 Organic aerosol density

In the chamber DWARF model, the $ALWC$ is determined by the aerosol volume (constrained to SMPS measurements) and the aerosol mass concentration (typically taken from measurements by the aerosol mass spectrometer (AMS)). As shown in Eq. 10, this method requires information on the density of the organic fraction of the aerosol (Kroll et al., 2006). MECCA_CHAMEXP uses two approaches for estimating the density of an organic species in the aqueous phase.

The first approach uses pre-estimated densities derived by the UManSysProp tool previously published by Topping et al. (2016). This tool is a code framework for estimating physico-chemical properties of organic compounds based on a collection of group contribution methods. For each organic molecule, the corresponding SMILES string (Weininger, 1988) needs to be provided allowing identification of the chemical structure. The density of a specific compound ($\rho_{org(i)}$) is derived by combining several estimation schemes in UManSysProp. Based on the tests by Barley et al. (2013) and Topping et al. (2016), we selected a combination of methods developed in Poling et al. (2001) and Nannoolal et al. (2004). The scheme by Nannoolal et al. (2004) is applied to derive the boiling point and the critical temperature of the compounds. It uses a group contribution method with 207 predefined groups to derive the boiling point (T_b). The critical temperature (T_C), critical pressure, and critical volume are then estimated using an empirical parameterisation dependent on T_b, the molar mass, and the number of hydrogen atoms in the compound. A more detailed description is beyond the scope of this work. Further information can be found in Barley et al. (2013). The method in Poling et al. (2001) is used for estimating the density of deliquescent particles. Similar to the method in Nannoolal et al. (2004), a group contribution method is applied that uses predefined functional elements to derive the molar volume. Finally, the estimated properties and the Rackett Equation (liquid density calculation, Rackett (1970)) are used to calculate the desired density (Poling et al., 2001).

The second method is the simpler density calculation by Kuwata et al. (2012), which uses the hydrogen-to-carbon (H/C) and oxygen-to-carbon (O/C) ratios of a specific molecule (Eq. 14).

$$\rho_i^{org} = \frac{12 + (H/C)_i + 16 \cdot (O/C)_i}{7 + 5 \cdot (H/C)_i + 4.15 \cdot (O/C)_i} \tag{14}$$

where ρ_i^{org} ($\mathrm{g\,cm^{-3}}$) is the density of an organic species, and H, C and O are the numbers of hydrogen, carbon and oxygen atoms of that species.

Additionally, the oxygen-to-carbon ratio and hydrogen-to-carbon ratio are indicators for the oxidation state of the organic aerosol (OA). In MECCA-CHAMEXP, the mean oxygen-to-carbon ratio ($\overline{\mathrm{O/C}}$) and hydrogen-to-carbon ratio ($\overline{\mathrm{H/C}}$) are calculated as below:

$$\overline{O/C} = \frac{\sum \left(C_{org[i]} \cdot (O/C)_i\right)}{C_{OA}} \tag{15}$$

$$\overline{H/C} = \frac{\sum \left(C_{org[i]} \cdot (H/C)_i\right)}{C_{OA}} \tag{16}$$

https://doi.org/10.5194/egusphere-2026-4522
Preprint. Discussion started: 13 August 2026

The ratios are averages weighted by the concentrations of each organic species. Consistently with AMS measurements, the oxygen atoms of nitrogen-containing functional groups are excluded.

5.2 Exchanges of gases with the walls

The gas partitioning to the particle phase is in competition with the loss of gas-phase species to the surface of the chamber wall. The loss rate due to gas-wall partitioning depends on several factors, including the properties of the wall material, the ratio of the chamber volume to its surface area, the chemical properties of the organic compounds, the turbulent mixing of the air, the temperature and the relative humidity. Therefore, the loss rates observed may vary significantly between different chambers and between experiments. Consequently, when simulating chamber experiments, it is recommended to use a specific gas-wall loss rate for each experiment. The gas-wall exchanges are implemented by adding an "aerosol mode" that represents the chamber wall (Sect. S1.4.1.). The wall exchanges for each organic species critically depend on the estimated volatility.

MESSy is designed as an atmospheric model and includes properties of the compounds such as Henry's law constants. The same wall loss and wall emission rates are applied for species with a similar volatility. Therefore, a conversion of Henry's law constants to the volatility of organic compounds is necessary. The work of Hodzic et al. (2014) provides a correlation between the effective Henry's law constant (H) and the volatility (C^*) (Donahue et al., 2009) of oxidation products for eight organic precursor classes and for two NO_x levels each. The user can choose the precursor class via the namelist. The appropriate $C^* - H$ relationship is then selected at each time step depending on the simulated NO_x level.

The partitioning of a species (X) between the gas phase and the chamber wall is described by the wall loss rate constant $k_{f,wall}$, while the outgassing from the chamber wall is determined by the wall emission rate constant $k_{b,wall}$ (s^{-1}). Following the definitions in Donahue et al. (2009), the gaseous organic species are grouped into the following categories:

- Extremely low volatility organic compounds (ELVOCs): $C^* \leq 10^{-4}$ µg m^{-3}.
- Low volatility organic compounds (LVOCs): 10^{-4} µg m^{-3} $< C^* \leq 0.1$ µg m^{-3}.
- Semi-volatile organic compounds (SVOCs): 0.1 µg m^{-3} $< C^* \leq 100$ µg m^{-3}.
- Intermediate volatility organic compounds (IVOCs): 100 µg m^{-3} $< C^* \leq 10^6$ µg m^{-3}.

As the gas-wall exchange rates vary between different experiments or chambers, users are able to set the $k_{f,wall}$ and $k_{b,wall}$ via the namelists of the MECCA submodel. In addition, default values can be set using gas-wall loss rates determined in a Teflon chamber with a volume range of 6–20 m^3 given by Krechmer et al. (2020).

https://doi.org/10.5194/egusphere-2026-4522
Preprint. Discussion started: 13 August 2026

6 Model evaluation

In order to validate and optimize the chamber DWARF, experiments from three environmental chambers were simulated. Firstly, to test the performance of the chamber DWARF with respect to gas-phase chemistry, an oxidation experiment with a terpenoid (2-methyl-3-butene-2-ol, MBO) carried out in the SAPHIR chamber (Novelli et al., 2018) is simulated. Secondly, a test experiment with hydrogen peroxide in the BATCH chamber (Löher et al., 2024) is modeled . Finally, the phase partitioning and the wall losses are tested by simulating the oxidation of α-pinene with seed particles in a SAPHIR-STAR experiment (Baker et al., 2024). In this work, the exchanges of trace gases with the chamber wall are implemented only in the simulation of the experiment in the SAPHIR-STAR chamber, as the wall loss rates were experimentally determined.

6.1 Gas-phase oxidation of MBO in the SAPHIR chamber

In order to test the chamber DWARF, simulated trace gases and radical concentrations are compared to observations. The study of the OH oxidation of MBO in the SAPHIR chamber by Novelli et al. (2018) was selected for this evaluation. A broad range of trace gases and radical concentrations were measured. Figure 5 shows the time series of the trace gases from the experiment. At the start of the experiment, the chamber contained only synthetic air. Water vapour was injected into the dark chamber via a carrier flow of synthetic air until a concentration of approximately $5 \times 10^{17}\,\mathrm{cm}^{-3}$ was reached. Ozone, generated by a silent discharge ozonizer (O3onia), was injected to reach a mixing ratio of $40\,\mathrm{nmol\,mol}^{-1}$. This period is referred to as the dark phase of the experiment. Upon opening the chamber shutter system, nitrous acid (HONO) was photochemically produced on the Teflon surfaces and released into the chamber air. During the period with opened roof, MBO was injected three times to reach mixing ratios of approximately $4\,\mathrm{nmol\,mol}^{-1}$.

A simulation with the MOM mechanism in the DWARF model was performed for this experiment. For comparability with the simulation by Novelli et al. (2018), the MCM alkyl nitrate yield of the first-generation RO_2 was adopted. In the DWARF simulation, the physical parameters, including temperature, relative humidity, pressure, the solar zenith angle (SZA) and the dilution rate were constrained to measured data. The photolysis frequencies of O_3, NO_2, H_2O_2, HONO, HCHO and other oxygenated volatile organic compound (VOC) were constrained to calculations using the measured solar actinic flux. Concentrations of HONO, NO, and NO_2 were also constrained to the measurements in both simulations. Wall emissions of HONO, HCHO and acetone (details in Sect. S2.) and wall loss of O_3 were included in both simulations. The injection of O_3 and the three injections of MBO were modeled by point-in-time injections.

The results of the "MOM-DWARF" simulation are compared to the observations and box model simulations "MCM-EASY" performed by Novelli et al. (2018) in Fig. 5. The MOM-DWARF simulation well reproduced the measured concentrations of OH before and after injection of MBO. However, similar to "MCM-EASY", HO_2 is

https://doi.org/10.5194/egusphere-2026-4522
Preprint. Discussion started: 13 August 2026

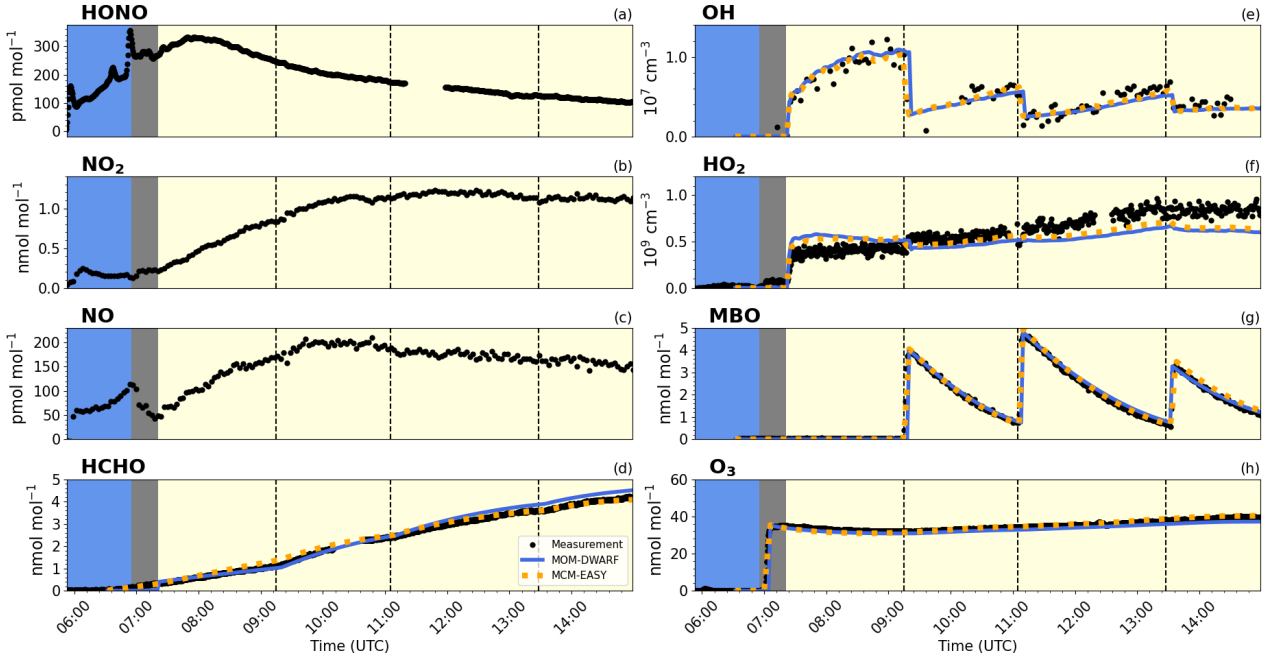

Figure 5. Modeled and measured time series of trace gases of the MBO photooxidation experiment conducted in the SAPHIR chamber. Measured data are compared to the results of two simulations using MOM in MESSy DWARF with reduced alkyl nitrate yield (MOM-DWARF, blue solid line), MCM in EASY (MCM-EASY, yellow dotted line; Novelli et al. (2018)). Water vapor was injected into the chamber at the beginning (blue shaded area). O_3 was injected when the chamber roof was closed (gray shaded area). During the time, when the chamber roof was open (yellow area), MBO was injected three times and oxidised by OH.

overpredicted before and underpredicted after the MBO injection. The reasons for the discrepancy are not clear. Nevertheless, both simulations reproduced well O_3.

6.2 Test experiment in the BATCH chamber

The chamber DWARF was tested for an experiment in the Teflon chamber BATCH at University of Bayreuth, Germany. The model set-up was the same as for the simulation of the SAPHIR experiment, but the dilution rate was set to zero because this chamber is operated without a replenishment flow. The BATCH chamber is made of Teflon, which is similar to the SAPHIR chamber, so that also emissions of compounds from the chamber wall like HONO are expected. However, the BATCH chamber wall emissions are not characterised. Therefore, wall emissions were set to zero and the effects of wall emissions were excluded from this test. The simulated experiment was a first test experiment for the chamber after it had been equipped with a new Teflon film. In the experiment, the chamber was first flushed with synthetic air, followed by the introduction of hydrogen peroxide (H_2O_2) in a carrier

https://doi.org/10.5194/egusphere-2026-4522
Preprint. Discussion started: 13 August 2026

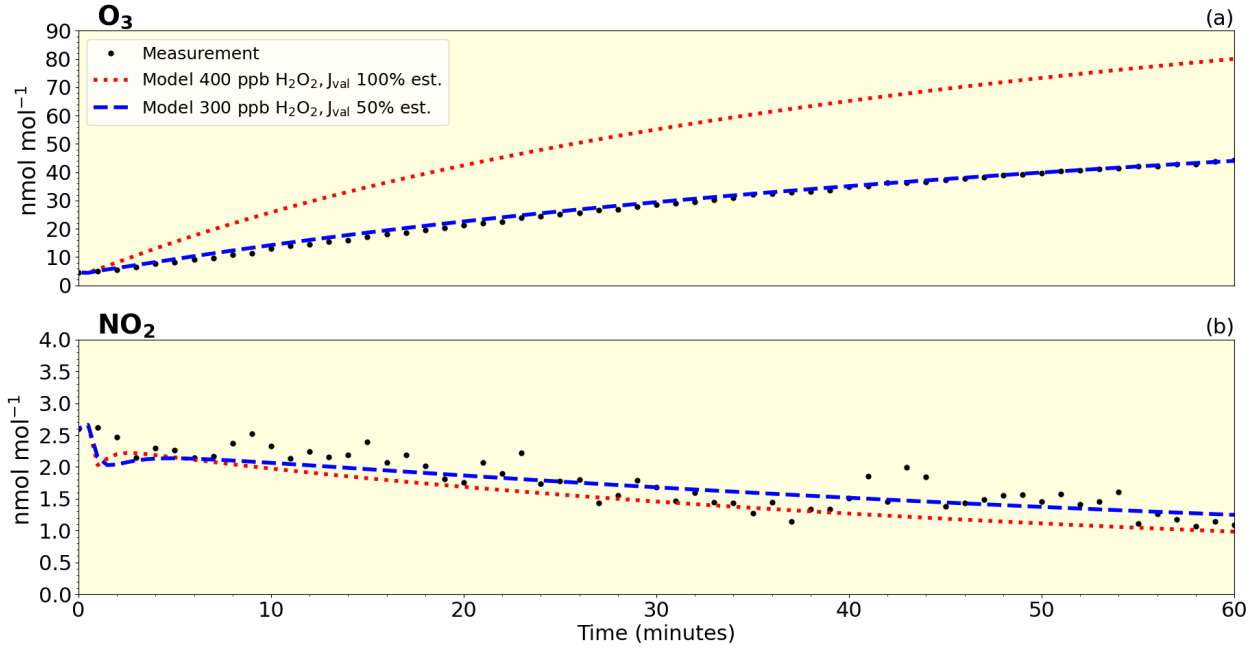

Figure 6. Modeled and measured time series of NO_2 and O_3 during a test experiment (25 June 2024), where H_2O_2 was photolysed in the BATCH chamber. Two simulations with different photolysis frequencies (100% and 50% of the estimated value) and different H_2O_2 levels were conducted.

flow of N_2. Subsequently, the lamps were turned on for one hour. During the experiment, the concentrations of O_3, NO_2 and NO were monitored. However, the NO measurements showed very large scatter and no clear trend (mean: 2.7 nmol mol^{-1}).

Figure 6 presents the comparison between observations and model simulations of NO_2 and O_3. Two different simulations were performed. In the first simulation, model input values were based on expectations from the experimental procedure, which are 100 % of the photolysis frequencies reported by the chamber operators and 400 nmol mol^{-1} H_2O_2. This simulation resulted in O_3 concentrations approximately twice as high as the measurements, while NO_2 was slightly underpredicted. In the second simulation with 50 % of the photolysis frequencies and a H_2O_2 mixing ratio of 300 nmol mol^{-1}, the model was able to reproduce the observed O_3 production and NO_2 decay reasonably well.

The estimated uncertainty range for the photolysis frequencies calculated by Löher et al. (2024) was ±38 %, and the expected H_2O_2 mixing ratio was between 400 and 500 nmol mol^{-1}. The model simulations suggest that the estimated boundary conditions are not consistent with the observations. The model configuration required H_2O_2 concentrations and/or photolysis frequencies, which are outside of the expected uncertainties ranges to produce an acceptable model-measurement agreement for ozone. These results suggest that either the photolysis frequencies or

https://doi.org/10.5194/egusphere-2026-4522
Preprint. Discussion started: 13 August 2026

the actual H_2O_2 concentration in the chamber may have been lower than the original assumptions. Uncertainties in the photolysis frequencies may be due to ageing of the UV-C lamps since the last spectral characterisation of the chamber or different optical properties of the new Teflon film. In terms of the H_2O_2 concentration, the calculation of the introduced H_2O_2 may not be fully transferable between different studies and chambers, for instance owing to changes in the efficiency of enriching the N_2 flow at different flow rates. The model simulation can help identifying these limitations.

6.3 α-pinene oxidation with seed aerosol in the SAPHIR-STAR chamber

The model representation of the aqueous aerosol phase enables the chamber DWARF to simulate photooxidation experiments with seed aerosol at moderate or high humidity. An experiment studying the photooxidation of α-pinene in the presence of ammonium sulfate seed aerosol in the SAPHIR-STAR chamber is used to test the chamber DWARF's capability to simulate the partitioning of gas-phase species to the particle phase (Fig. 4). In this experiment, α-pinene, O_3, NO, and seed aerosol were injected into the chamber at a constant rate to reach steady-state concentrations. Throughout the experiment, the temperature and relative humidity remained constant, while the injection rates of O_3 were changed three times (Tab. 3).

Table 3: Conditions for the three steady-states of α-pinene photooxidation in the SAPHIR-STAR chamber. The temperature and relative humidity were constant with values of 295 K and 50 %. $VOC_{[in]}$ and $O_{3[in]}$ represent the measured mixing ratio of α-pinene and O_3 in the chamber before reactions. The $O_{3[ss]}$, $NO_{[ss]}$, $NO_{x[ss]}$ mixing ratios, and the particle number concentration were measurements during steady-state conditions of the experiment.

Steady-state phase	$VOC_{[in]}$ ($nmol\,mol^{-1}$)	$O_{3[in]}$ ($nmol\,mol^{-1}$)	$O_{3[ss]}$ ($nmol\,mol^{-1}$)	$NO_{[in]}$ ($nmol\,mol^{-1}$)	$NO_{[ss]}$ ($nmol\,mol^{-1}$)	$NO_{x[ss]}$ ($nmol\,mol^{-1}$)	Particle number concentration ($\#\,cm^{-3}$)
1 (High NO)	10	46.0	33.3	25	0.5	9.1	55000
2 (Medium NO)	10	36.0	28.4	10	0.3	3.7	58000
3 (Low NO)	10	34.0	26.0	3.4	0.2	1.4	60000

In order to evaluate the multi-phase partitioning scheme a number of parameters in chamber DWARF were constrained to the measurements. Firstly, aerosol properties including the number concentration, the mean diameter of particle size distribution, the standard deviation of the particle log-normal size distribution, and the inorganic ion mass concentrations (SO_4^{2-}, NO_3^-, NH_4^+) were constrained to observations for the calculation of $ALWC$. Secondly, the time series of gaseous species (α-pinene, ozone, NO, NO_2) were constrained to measurements in order to avoid that model-measurement discrepancies of gas-phase species affected the prediction of the secondary organic mass. Finally, the photolysis frequencies of O_3 and NO_2 determined in previous actinometry experiments were used. With a flow of $32\,L\,min^{-1}$ the residence time in the SAPHIR-STAR chamber was approximately 60 minutes. The respective flow was described in the model by applying a first-order loss reaction for each individual chemical species with a constant rate of $2.67 \times 10^{-4}\,s^{-1}$.

https://doi.org/10.5194/egusphere-2026-4522
Preprint. Discussion started: 13 August 2026

6.3.1 Organic aerosol mass concentration and gas wall loss

In a previous study, Baker et al. (2024) reported a wall-loss rate coefficient of $5.88 \times 10^{-3}\,s^{-1}$ for highly oxygenated molecules (HOM) and RO_2 radicals in the SAPHIR-STAR chamber. In this experiment, the IVOCs and SVOCs produced from the photooxidation of α-pinene were regarded as highly volatile species with a low potential for partitioning into the particle phase. Therefore, the wall loss of IVOCs and SVOCs was assumed to be negligible. On the orther hand, as HOMs are expected to be low volatile and their the wall-loss rates used for all species falling into the ELVOCs and LVOCs categories. The wall-loss rates of HOMs and RO_2 radicals reported in the previous work were used.

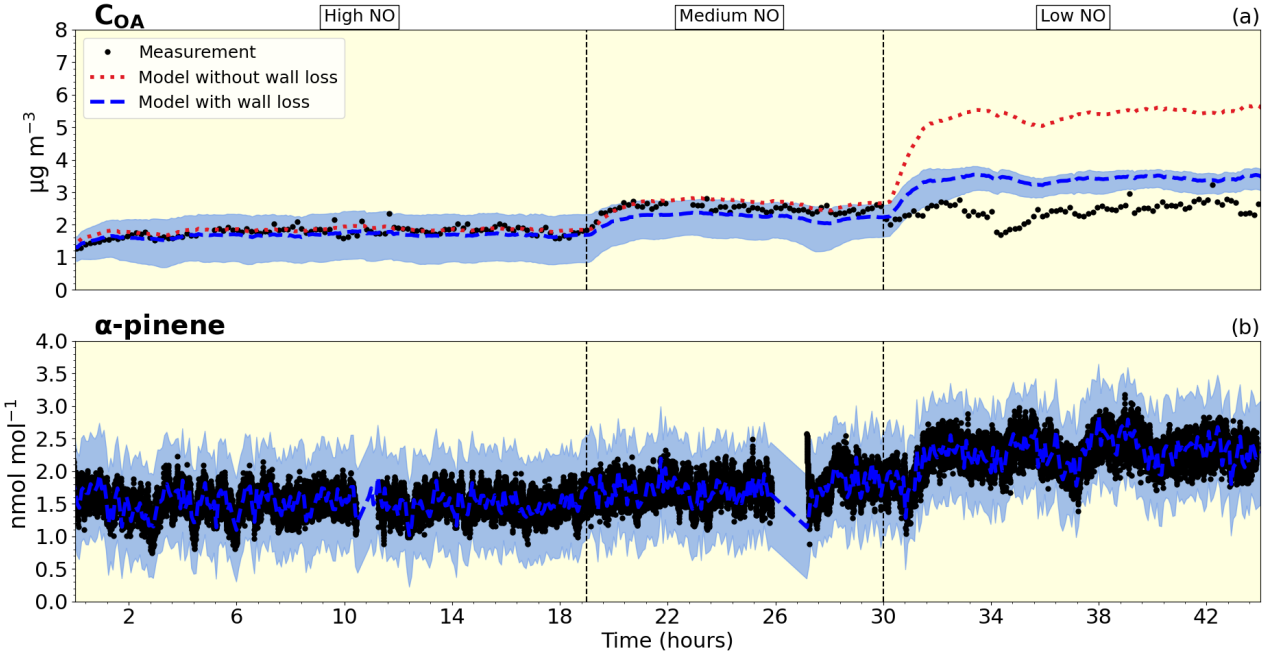

Figure 7. Modeled and measured time series of: a) the organic aerosol mass concentration (model with and without wall loss) and b) α-pinene. The blue shaded area shows the model uncertainty based on 5 minutes interval of sample standard deviation performed on α-pinene observation. There are three steady-state phases in the experiment named high, medium and low NO (Tab. 3)

.

To demonstrate the impact of the gas wall-loss process on the prediction of total organic mass in the particle phase, two simulations of the α-pinene photooxidation experiment were conducted, one with and one without including the wall loss of gaseous species. Figure 7 compares the organic mass concentration in the aqueous aerosol phase derived from measurements and the two simulations. In both simulations, the time series of α-pinene, NO_x, O_3, and particle properties (number concentration, mean diameter of particle size distribution , inorganic aerosol mass concentration)

https://doi.org/10.5194/egusphere-2026-4522
Preprint. Discussion started: 13 August 2026

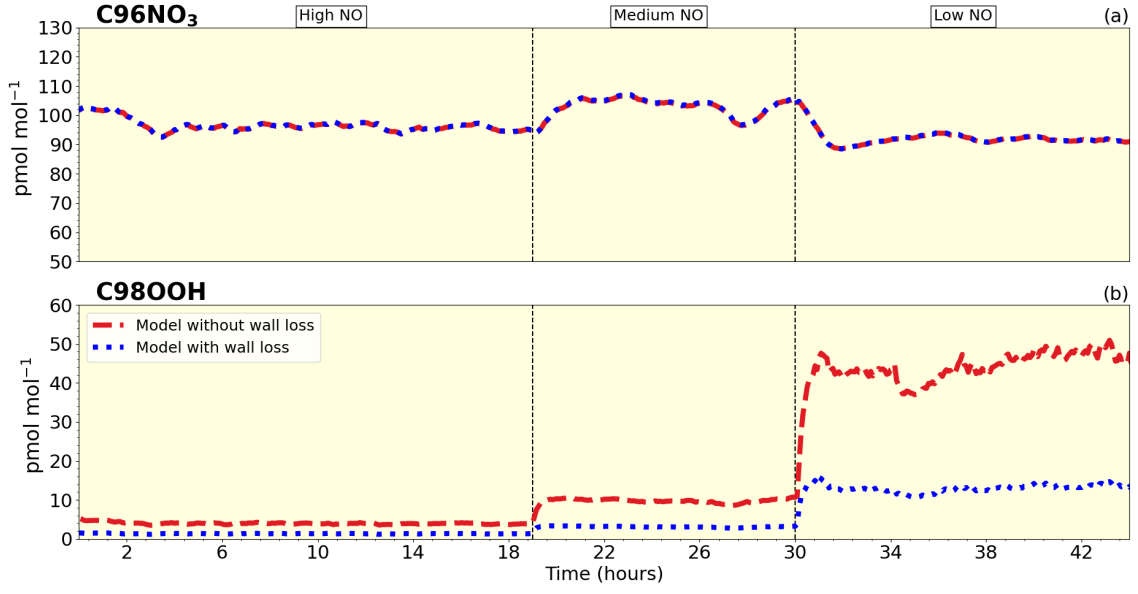

Figure 8. Simulated time series of two α-pinene oxidation products in the gas phase: a) C96NO3 and b) C98OOH. Simulation results with and without wall loss are shown. Only the low volatile species C98OOH is affected by loss to the walls.

were constrained to observational data, averaged over a five-minute time interval. At the highest level of NO_x, the inclusion of the wall loss in the model results in a ≈3-5 % lower organic mass than in the model run without wall loss. However, results of both simulations agree within the uncertainty range of the measurements. At medium NO_x level, the simulated organic mass is approximately 10 % lower in the simulation including wall loss compared to without wall loss. However, the predictions by both models still remain within the uncertainty range of the measurement. In contrast, for the lowest NO_x condition, the simulation without gas-wall partitioning predicts almost twice as high as the observed organic mass concentration. If wall loss is included, however, the model results show a significant better agreement with the measurements. The slightly higher prediction of the organic mass during the third phase of the experiment could be attributed to the production of more highly soluble species under lower NO_x conditions in the used chemical mechanism (MOM). The organonitrates, formed preferably at high-NO_x conditions, typically have a lower solubility than the species with carboxyl and hydroxyl functional groups, which are preferably formed under low NO_x conditions (Suda et al., 2014).

To further investigate gas-wall loss effects on the organic mass prediction, Fig. 8 shows the time series of two products from an α-pinene photoxidation. One product, $C96NO_3$, contains a nitrate functional group and the other product, C98OOH, contains a carboxyl functional group. These names, and the later products names, are chemical compound identifiers utilized for atmospheric chemical models in the MCM. The chamber DWARF partitioning scheme categorizes organic species into different volatility groups (Sec. 5.2). $C96NO_3$ is categorized as highly volatile and thus, it is considered as being less likely lost to chamber walls. On the other hand, C98OOH is classified as a low

https://doi.org/10.5194/egusphere-2026-4522
Preprint. Discussion started: 13 August 2026

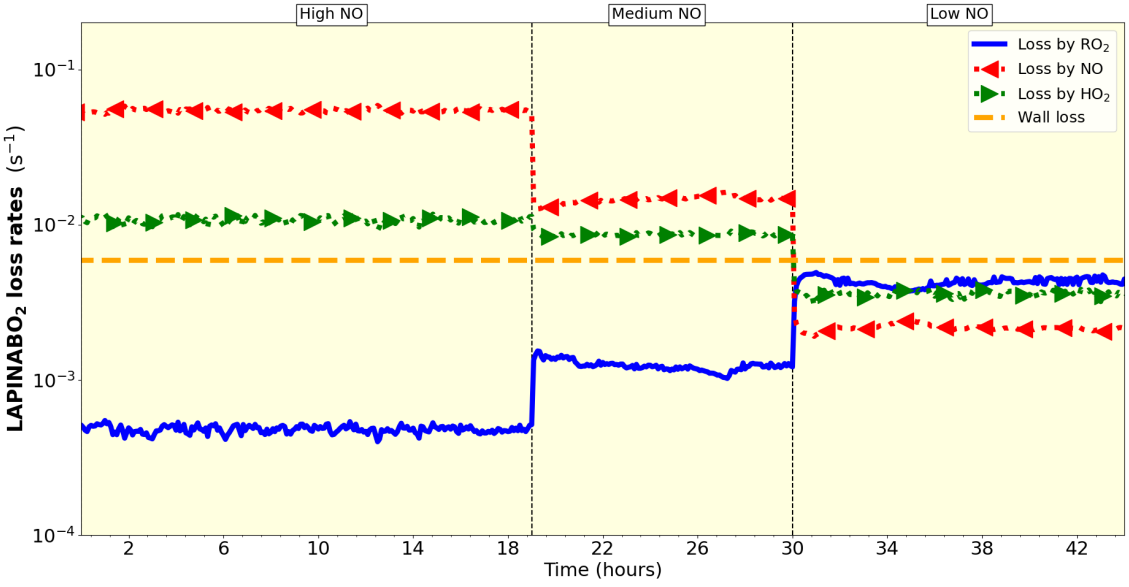

Figure 9. Modeled loss rates of the RO_2 radical LAPINABO$_2$ formed in the reaction of α-pinene with OH due to its reactions with other RO_2 radicals, NO, HO_2 and due to wall loss.

volatile compound, which has a significant loss to the chamber wall. Thus, the simulations with and without wall loss show the same concentrations for C96NO$_3$. However, there is a large effect of the wall loss on the concentration of C98OOH. The differences between the predicted concentrations of C98OOH in the two simulations are consistent with the differences in the predicted organic mass. In fact, organic hydroperoxides like C98OOH generally have larger Henry's law coefficients (smaller volatility) than organic nitrates.

Figure 9 shows the loss rate of the lumped first-generation RO_2 radicals from the OH-reaction of α-pinene, LAPINABO$_2$ in the reactions with RO_2, NO, HO_2 and its interaction with the chamber wall due to wall loss (Section 5.2) in the model. At the highest NO level of 0.5 nmol mol^{-1}, the loss rate of LAPINABO2 in the reaction with NO is highest (around 6×10^{-2} s^{-1}) compared to loss to other reactions. When the NO mixing ratio is 0.3 nmol mol^{-1} in the second phase of the experiment, the loss rates of LAPINABO2 in the reaction with NO, and HO_2 decreased to around 1×10^{-2} s^{-1}. At the lowest NO level of 0.2 nmol mol^{-1}, the loss rates of LAPINABO2 in the reaction with RO_2 and HO_2 are around 4×10^{-3} s^{-1} which is two times higher than that in the reaction with NO. These results agree with the previously shown increases in the formation of C98OOH, which is a product of $RO_2 + HO_2$ reactions. The loss rate of LAPINABO2 due to interaction with the chamber wall is comparable with its loss due to chemical reactions. However, the overall RO_2 loss to the chamber wall has a minor impact on the organic mass formation. In a specific simulation in which the gas-wall loss of ELVOCs and LVOCs was deactivated and the wall loss of RO_2 was maintained the outcomes demonstrated a negligible difference in the organic mass.

https://doi.org/10.5194/egusphere-2026-4522
Preprint. Discussion started: 13 August 2026

6.3.2 Prediction of the aerosol liquid water content

One approach to calculate $ALWC$ is using the aerosol hygroscopic growth factor. From a previous study by Varutbangkul et al. (2006); Petters and Kreidenweis (2007), the growth factor of products from α-pinene is around 1 to 2 % which is relatively low in comparison to the value of ammonium sulfate. Therefore, in this study, it is assumed that the growth factor of the organic component is 1.0 and that water uptake in the aqueous phase was predominantly driven by the inorganic seeds. The growth factor of ammonium sulfate is estimated by fitting parameters from the work of Kreidenweis et al. (2005) (Sect. S1.4.2.) for particles at a temperature of 295 K.

Figure 10 (a) and (b) illustrate the comparison of the $ALWC$ prediction in two model simulations using the two implemented methods, introduced in Sect. 5.1.1, and their effect on the prediction of the secondary organic mass. The unit $ALWC$ is converted to $\mu g\,m^{-3}$ for compatibility with organic mass concentration. The simulation results indicate a relatively stable $ALWC$ during the experiment. As the exchange coefficient of water-soluble species to the particle phase depends on the $ALWC$, the predicted organic mass in the aqueous phase increases with increasing $ALWC$. The model predicted the O/C ratio of organic matter in the aqueous phase to be approximately 0.6 under high NO_x conditions, which agrees well with the measurements. Even though the model slightly overpredicted the O/C ratio at lower NO_x conditions, it captured the decreasing trend observed in the measurements (Fig. 10 c).

These results are consistent with the organic mass prediction discussed above, showing that the decrease in the NO_x level was accompanied by a decline in the concentration of the predominant organic nitrate species. At the same time, the formation of other species bearing carboxyl and hydro(pero)xyl functional groups was favoured. It should be noted that the measurement of the O/C ratio by the AMS instrument does not account for the oxygen contained in the nitrate group. Thus, the measured O/C ratio for organic nitrates is lower compared to carboxyl and hydroxyl species. The variation in the O/C ratio over the course of the experiment influenced the mean organic matter density, which was calculated using the elements method based on the H/C and O/C ratios (Fig. 10 d). As the O/C ratio decreased, the average density of the organic components also decreased. Although this trend is observable in the density calculated by the UManSysProp method as well, it is not significant. In general, the element method estimated the mean density of organic components to be approximately $1.4\,g\,cm^{-3}$ and $1.3\,g\,cm^{-3}$ at the highest and lowest NO_x level, respectively. In contrast, the UManSysProp method yielded a relatively constant density throughout the experiment, with a mean value of approximately $1.2\,g\,cm^{-3}$. The mean aerosol density, as predicted by both methods, formed from α-pinene photooxidation in an experiment with seed aerosol is expected to range between 1.4 and $1.6\,g\,cm^{-3}$ (Fig. S5), which is consistent with the findings of a previous study (Kostenidou et al., 2007). Despite a 15 % discrepancy in the average organic density, the average aqueous densities estimated by the two methods are relatively similar. This can be explained by the low mass fraction of organic material (approximately 16 %) present in the particle phase. Therefore, the effect on the overall density of the aqueous aerosol phase is minimal.

https://doi.org/10.5194/egusphere-2026-4522
Preprint. Discussion started: 13 August 2026

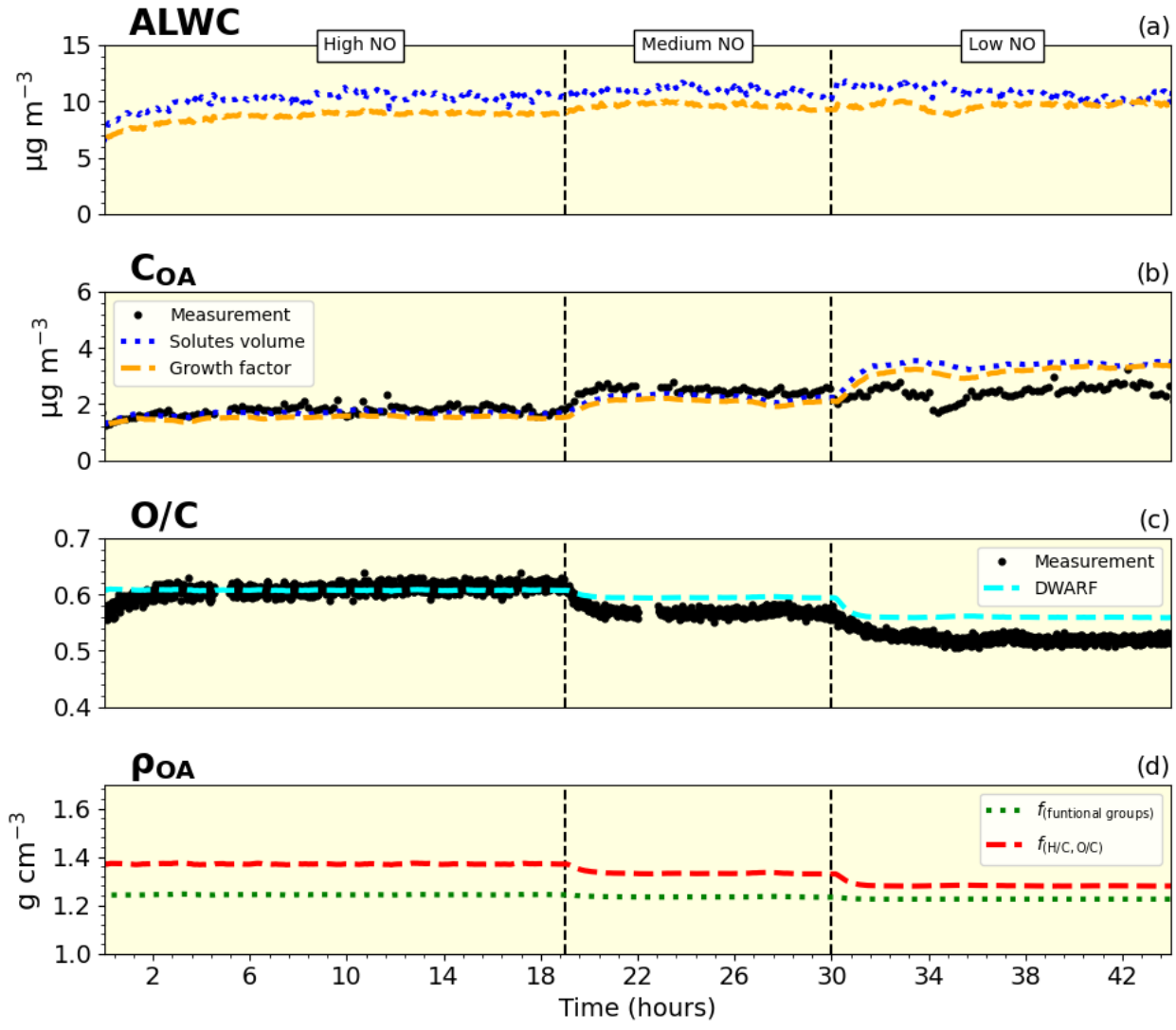

Figure 10. Time series comparing the different approaches to estimate the aerosol $ALWC$ and the organic aerosol density in the model using: a) the liquid water content and b) the associated organic aerosol mass concentration calculated using two approaches: the solutes volume and the aerosol hygroscopic growth factor, c) comparison of the O/C ratio from model result and AMS measurements, d) the organic aerosol density estimated based on: The UManSysProp approach and using the H/C and O/C ratios.

7 Summary and outlook

In this work, the MESSy-based chemical box model setup "chamber DWARF" for simulating atmospheric chamber experiments is described. We present how to configure the MESSy DWARF model as a box model to simulate

https://doi.org/10.5194/egusphere-2026-4522
Preprint. Discussion started: 13 August 2026

chamber experiments, using the advantages of MESSy's infrastructure. By selecting individual MESSy submodels, we adapted the model to different experimental setups. Each submodel handled one or more processes during a chamber experiment.

We tested the chamber DWARF by comparing model results with observations from experiments in three different chambers. In an experiment on the OH oxidation of MBO in the SAPHIR chamber, DWARF reproduced trace gas and radical concentrations. We also used the model to optimize the description of chamber effects, as shown by the experiment in the BATCH chamber. In the SAPHIR-STAR chamber, we evaluated the multi-phase partitioning scheme using an α-pinene photooxidation experiment with ammonium sulfate seed aerosol. The results confirmed the effectiveness of the kinetic partitioning scheme based on the liquid water content and water solubility (from Henry's law coefficients). The model matched the observed organic aerosol mass concentrations.

We further investigated how gas-phase wall loss affected the predicted organic aerosol mass concentration. As expected, the model shifted the organic aerosol mass from nitrate functional groups toward carboxyl and hydro(pero)xyl functional groups as NO decreased. In the model, this shift increased the influence of wall loss on the overall organic mass formed in the aqueous phase. This occurred because, in the employed partitioning scheme, carboxyl- and hydroxyl-containing species classified as low volatile compounds exhibited higher wall loss rates.

Chamber DWARF provides two methods to estimate aerosol liquid water content: solute volume and the hygroscopic growth factor. Model predictions showed a discrepancy of about 20 % between the two approaches. The model also provides two methods to calculate the mean organic mass density: using the H/C and O/C element ratios or using UManSysProp. Although the element-ratio method produced a higher organic density than UManSysProp, the discrepancy did not affect the mean aerosol density because the organic mass fraction remained small in the example experiment.

This evaluation demonstrated the strong potential of simulating chamber experiments with the MESSy chamber DWARF setup. Future work will extend the capabilities for multi-phase chemistry in chamber experiments. We will represent specific chamber processes and extend the kinetic model. In particular, we will improve liquid water content estimates from growth factors, refine chamber wall losses using state-of-the-art volatility estimates, and better represent partitioning and aging of organic vapors in the condensed phase.

Code and data availability. The Modular Earth Submodel System (MESSy) is being continuously further developed and applied by a consortium of institutions. The usage of MESSy and access to the source code is licenced to all affiliates of institutions who are members of the MESSy Consortium. Institutions can become a member of the MESSy Consortium by signing the MESSy Memorandum of Understanding. More information can be found on the MESSy Consortium website (http://www.messy-interface.org, last access: 15th July 2026). The simulations results presented here have been performed with the code archived with DOI https://doi.org/10.5281/zenodo.21526582 (The MESSy Consortium, 2026). This code can also be accessed by the editor and the reviewers. The scripts for plotting and creating the input data are available at https://doi.org/10.5281/zenodo.21529803. The data used for the plots are available at https://doi.org/10.5281/zenodo.21533206.

https://doi.org/10.5194/egusphere-2026-4522
Preprint. Discussion started: 13 August 2026

Author contributions. DHD developed MESSy DWARF to simulate chamber experiments, and wrote the largest part of manuscript and the Supplement. DT contributed in conceptualization, methodology, formal analysis, writing - review & editing manuscript. AK supervised the development, writing-review & editing manuscript. FW provided and wrote the estimation of organic density. AP and ND developed auto-generation and plotting scripts. HF, BB and AN provided data and input for simulating SAPHIR chamber. FL and ACN provided data and input for simulating BATCH chamber. YB and SZ provided data and input for simulating SAPHIR-STAR chamber. All authors provided feedback on the manuscript and have given approval to the final version.

Competing interests. The co-author A. Kerkweg is executive editor of the GMD journal.

Acknowledgements. We thank Jan Hegi, Maximilian Striegel and Gereon Vincenti for their work on the chamber visualization tool as part of the software engineering project at the FH Aachen.

https://doi.org/10.5194/egusphere-2026-4522
Preprint. Discussion started: 13 August 2026

References

Baker, Y., Kang, S., Wang, H., Wu, R., Xu, J., Zanders, A., He, Q., Hohaus, T., Ziehm, T., Geretti, V., Bannan, T. J., O'Meara, S. P., Voliotis, A., Hallquist, M., McFiggans, G., Zorn, S. R., Wahner, A., and Mentel, T. F.: Impact of HO2/RO2 ratio on highly oxygenated α-pinene photooxidation products and secondary organic aerosol formation potential, Atmospheric Chemistry and Physics, 24, 4789–4807, https://doi.org/10.5194/acp-24-4789-2024, 2024.

Barley, M. H., Topping, D. O., and McFiggans, G.: Critical Assessment of Liquid Density Estimation Methods for Multifunctional Organic Compounds and Their Use in Atmospheric Science, The Journal of Physical Chemistry A, 117, 3428–3441, https://doi.org/10.1021/jp304547r, 2013.

Bohn, B. and Zilken, H.: Model-aided radiometric determination of photolysis frequencies in a sunlit atmosphere simulation chamber, Atmospheric Chemistry and Physics, 5, 191–206, https://doi.org/10.5194/acp-5-191-2005, 2005.

Bohn, B., Rohrer, F., Brauers, T., and Wahner, A.: Actinometric measurements of NO_2 photolysis frequencies in the atmosphere simulation chamber SAPHIR, Atmospheric Chemistry and Physics, 5, 493–503, https://doi.org/10.5194/acp-5-493-2005, 2005.

Cabrera-Perez, D., Taraborrelli, D., Sander, R., and Pozzer, A.: Global atmospheric budget of simple monocyclic aromatic compounds, Atmospheric Chemistry and Physics, 16, 6931–6947, https://doi.org/10.5194/acp-16-6931-2016, 2016.

Donahue, N. M., Robinson, A. L., and Pandis, S. N.: Atmospheric organic particulate matter: From smoke to secondary organic aerosol, Atmospheric Environment, 43, 94–106, https://doi.org/10.1016/j.atmosenv.2008.09.055, 2009.

Franco, B., Blumenstock, T., Cho, C., Clarisse, L., Clerbaux, C., Coheur, P.-F., De Mazière, M., De Smedt, I., Dorn, H.-P., Emmerichs, T., Fuchs, H., Gkatzelis, G., Griffith, D. W. T., Gromov, S., Hannigan, J. W., Hase, F., Hohaus, T., Jones, N., Kerkweg, A., Kiendler-Scharr, A., Lutsch, E., Mahieu, E., Novelli, A., Ortega, I., Paton-Walsh, C., Pommier, M., Pozzer, A., Reimer, D., Rosanka, S., Sander, R., Schneider, M., Strong, K., Tillmann, R., Van Roozendael, M., Vereecken, L., Vigouroux, C., Wahner, A., and Taraborrelli, D.: Ubiquitous atmospheric production of organic acids mediated by cloud droplets, Nature, 593, 233–237, https://doi.org/10.1038/s41586-021-03462-x, 2021.

Fuchs, H., Hofzumahaus, A., Rohrer, F., Bohn, B., Brauers, T., Dorn, H.-P., Häseler, R., Holland, F., Kaminski, M., Li, X., Lu, K., Nehr, S., Tillmann, R., Wegener, R., and Wahner, A.: Experimental evidence for efficient hydroxyl radical regeneration in isoprene oxidation, Nature Geoscience, 6, 1023–1026, https://doi.org/10.1038/ngeo1964, 2013.

Fuchs, H., Illmann, N., Muñoz, A., Ródenas, M., Picquet-Varrault, B., Alfarra, M. R., Arsene, C., Bejan, I. G., Bell, D. M., Bilde, M., Böhmländer, A., Campos-Pineda, M., Cazaunau, M., Coll, P., Daële, V., Di Biagio, C., Flynn, M., Formenti, P., Herrmann, H., Höhler, K., Hohaus, T., Johnson, M. S., Juurola, E., Kivekäs, N., Kaiser, J., Kaltsonoudis, C., Laj, P., Massabò, D., Mazzei, F., McFiggans, G., McGillen, M. R., Mellouki, A., Mettke, P., Möhler, O., Mothes, F., Niedermeier, D., Novelli, A., Olariu, R. I., Pandis, S. N., Patroescu-Klotz, I., Petracca Altieri, R. M., Prati, P., Roman, C., Ruth, A. A., Saathoff, H., Schmalfuß, S., Stratmann, F., Vernocchi, V., Voliotis, A., Voigtländer, J., Virtanen, A., Wahner, A., Wagner, R., Wenger, J., Zorn, S., Wiesen, P., and Doussin, J.-F.: Atmospheric Simulation Chambers in the ACTRIS Research Infrastructure, Atmospheric Measurement Techniques, 19, 4165–4199, https://doi.org/10.5194/amt-19-4165-2026, 2026.

Hens, K., Novelli, A., Martinez, M., Auld, J., Axinte, R., Bohn, B., Fischer, H., Keronen, P., Kubistin, D., Nölscher, A. C., Oswald, R., Paasonen, P., Petäjä, T., Regelin, E., Sander, R., Sinha, V., Sipilä, M., Taraborrelli, D., Tatum Ernest, C.,

https://doi.org/10.5194/egusphere-2026-4522
Preprint. Discussion started: 13 August 2026

Williams, J., Lelieveld, J., and Harder, H.: Observation and modelling of HO_x radicals in a boreal forest, Atmospheric Chemistry and Physics, 14, 8723–8747, https://doi.org/10.5194/acp-14-8723-2014, 2014.

Hodzic, A., Aumont, B., Knote, C., Lee-Taylor, J., Madronich, S., and Tyndall, G.: Volatility dependence of Henry's law constants of condensable organics: Application to estimate depositional loss of secondary organic aerosols, Geophysical Research Letters, 41, 4795–4804, https://doi.org/10.1002/2014GL060649, 2014.

Jenkin, M. E., Saunders, S. M., and Pilling, M. J.: The tropospheric degradation of volatile organic compounds: a protocol for mechanism development, Atmospheric Environment, 31, 81–104, https://doi.org/10.1016/S1352-2310(96)00105-7, 1997.

Jöckel, P., Sander, R., Kerkweg, A., Tost, H., and Lelieveld, J.: Technical Note: The Modular Earth Submodel System (MESSy) - a new approach towards Earth System Modeling, Atmospheric Chemistry and Physics, 5, 433–444, https://doi.org/10.5194/acp-5-433-2005, 2005.

Jöckel, P., Kerkweg, A., Pozzer, A., Sander, R., Tost, H., Riede, H., Baumgaertner, A., Gromov, S., and Kern, B.: Development cycle 2 of the Modular Earth Submodel System (MESSy2), Geoscientific Model Development, 3, 717–752, https://doi.org/10.5194/gmd-3-717-2010, 2010.

Jöckel, P., Tost, H., Pozzer, A., Kunze, M., Kirner, O., Brenninkmeijer, C. A. M., Brinkop, S., Cai, D. S., Dyroff, C., Eckstein, J., Frank, F., Garny, H., Gottschaldt, K.-D., Graf, P., Grewe, V., Kerkweg, A., Kern, B., Matthes, S., Mertens, M., Meul, S., Neumaier, M., Nützel, M., Oberländer-Hayn, S., Ruhnke, R., Runde, T., Sander, R., Scharffe, D., and Zahn, A.: Earth System Chemistry integrated Modelling (ESCiMo) with the Modular Earth Submodel System (MESSy) version 2.51, Geoscientific Model Development, 9, 1153–1200, https://doi.org/10.5194/gmd-9-1153-2016, 2016.

Karl, M.: Modellierung atmosphärisch-chemischer Reaktionen in der Tageslicht-Atmosphären-Simulationskammer, Dr. (univ.), Univ. Münster, Jülich, ISSN 0944-2952, https://juser.fz-juelich.de/record/41885, record converted from VDB: 12.11.2012; Münster, Univ., Diss., 2004, 2004.

Kerkweg, A. and Jöckel, P.: The 1-way on-line coupled atmospheric chemistry model system MECO(n) – Part 1: Description of the limited-area atmospheric chemistry model COSMO/MESSy, Geoscientific Model Development, 5, 87–110, https://doi.org/10.5194/gmd-5-87-2012, 2012.

Kerkweg, A., Sander, R., Tost, H., Jöckel, P., and Lelieveld, J.: Technical Note: Simulation of detailed aerosol chemistry on the global scale using MECCA-AERO, Atmospheric Chemistry and Physics, 7, 2973–2985, https://doi.org/10.5194/acp-7-2973-2007, 2007.

Kerkweg, A., Kirfel, T., Do, D. H., Griessbach, S., Jöckel, P., and Taraborrelli, D.: The MESSy DWARF (based on MESSy v2.55.2), Geoscientific Model Development, 18, 1265–1286, https://doi.org/10.5194/gmd-18-1265-2025, 2025.

Kostenidou, E., , Ravi K., P., , and Pandis, S. N.: An Algorithm for the Calculation of Secondary Organic Aerosol Density Combining AMS and SMPS Data, Aerosol Science and Technology, 41, 1002–1010, https://doi.org/10.1080/02786820701666270, _eprint: https://doi.org/10.1080/02786820701666270, 2007.

Krechmer, J. E., Day, D. A., and Jimenez, J. L.: Always Lost but Never Forgotten: Gas-Phase Wall Losses Are Important in All Teflon Environmental Chambers, Environmental Science & Technology, 54, 12 890–12 897, https://doi.org/10.1021/acs.est.0c03381, 2020.

Kreidenweis, S. M., Koehler, K., DeMott, P. J., Prenni, A. J., Carrico, C., and Ervens, B.: Water activity and activation diameters from hygroscopicity data - Part I: Theory and application to inorganic salts, Atmospheric Chemistry and Physics, 5, 1357–1370, https://doi.org/10.5194/acp-5-1357-2005, 2005.

https://doi.org/10.5194/egusphere-2026-4522
Preprint. Discussion started: 13 August 2026

Kroll, J. H., Ng, N. L., Murphy, S. M., Flagan, R. C., and Seinfeld, J. H.: Secondary Organic Aerosol Formation from Isoprene Photooxidation, Environmental Science & Technology, 40, 1869–1877, https://doi.org/10.1021/es0524301, 2006.

Kuwata, M., Zorn, S. R., and Martin, S. T.: Using Elemental Ratios to Predict the Density of Organic Material Composed of Carbon, Hydrogen, and Oxygen, Environmental Science & Technology, 46, 787–794, https://doi.org/10.1021/es202525q, 2012.

Löher, F., Borrás, E., Muñoz, A., and Nölscher, A. C.: Characterization of a new Teflon chamber and on-line analysis of isomeric multifunctional photooxidation products, Atmospheric Measurement Techniques, 17, 4553–4579, https://doi.org/10.5194/amt-17-4553-2024, 2024.

Mallik, C., Tomsche, L., Bourtsoukidis, E., Crowley, J. N., Derstroff, B., Fischer, H., Hafermann, S., Hüser, I., Javed, U., Keßel, S., Lelieveld, J., Martinez, M., Meusel, H., Novelli, A., Phillips, G. J., Pozzer, A., Reiffs, A., Sander, R., Taraborrelli, D., Sauvage, C., Schuladen, J., Su, H., Williams, J., and Harder, H.: Oxidation processes in the eastern Mediterranean atmosphere: evidence from the modelling of HO_x measurements over Cyprus, Atmospheric Chemistry and Physics, 18, 10 825–10 847, https://doi.org/10.5194/acp-18-10825-2018, 2018.

Malm, W. C. and Kreidenweis, S. M.: The effects of models of aerosol hygroscopicity on the apportionment of extinction, Atmospheric Environment, 31, 1965–1976, https://doi.org/10.1016/S1352-2310(96)00355-X, 1997.

Nannoolal, Y., Rarey, J., Ramjugernath, D., and Cordes, W.: Estimation of pure component properties: Part 1. Estimation of the normal boiling point of non-electrolyte organic compounds via group contributions and group interactions, Fluid Phase Equilibria, 226, 45–63, https://doi.org/10.1016/j.fluid.2004.09.001, 2004.

Novelli, A., Kaminski, M., Rolletter, M., Acir, I.-H., Bohn, B., Dorn, H.-P., Li, X., Lutz, A., Nehr, S., Rohrer, F., Tillmann, R., Wegener, R., Holland, F., Hofzumahaus, A., Kiendler-Scharr, A., Wahner, A., and Fuchs, H.: Evaluation of OH and HO_2 concentrations and their budgets during photooxidation of 2-methyl-3-butene-2-ol (MBO) in the atmospheric simulation chamber SAPHIR, Atmospheric Chemistry and Physics, 18, 11 409–11 422, https://doi.org/10.5194/acp-18-11409-2018, 2018.

Novelli, A., Vereecken, L., Bohn, B., Dorn, H.-P., Gkatzelis, G. I., Hofzumahaus, A., Holland, F., Reimer, D., Rohrer, F., Rosanka, S., Taraborrelli, D., Tillmann, R., Wegener, R., Yu, Z., Kiendler-Scharr, A., Wahner, A., and Fuchs, H.: Importance of isomerization reactions for OH radical regeneration from the photo-oxidation of isoprene investigated in the atmospheric simulation chamber SAPHIR, Atmospheric Chemistry and Physics, 20, 3333–3355, https://doi.org/10.5194/acp-20-3333-2020, 2020.

Nölscher, A. C., Butler, T., Auld, J., Veres, P., Muñoz, A., Taraborrelli, D., Vereecken, L., Lelieveld, J., and Williams, J.: Using total OH reactivity to assess isoprene photooxidation via measurement and model, Atmospheric Environment, 89, 453–463, https://doi.org/10.1016/j.atmosenv.2014.02.024, 2014.

O'Meara, S. P., Xu, S., Topping, D., Alfarra, M. R., Capes, G., Lowe, D., Shao, Y., and McFiggans, G.: PyCHAM (v2.1.1): a Python box model for simulating aerosol chambers, Geoscientific Model Development, 14, 675–702, https://doi.org/10.5194/gmd-14-675-2021, 2021.

Petters, M. D. and Kreidenweis, S. M.: A single parameter representation of hygroscopic growth and cloud condensation nucleus activity, Atmospheric Chemistry and Physics, 7, 1961–1971, https://doi.org/10.5194/acp-7-1961-2007, 2007.

Poling, B. E., Prausnitz, J. M., O'connell, J. P., et al.: The properties of gases and liquids, vol. 5, Mcgraw-hill New York, 2001.

https://doi.org/10.5194/egusphere-2026-4522
Preprint. Discussion started: 13 August 2026

Rackett, H. G.: Equation of state for saturated liquids, Journal of Chemical and Engineering Data, 15, 514–517, 1970.

Raventos-Duran, T., Camredon, M., Valorso, R., Mouchel-Vallon, C., and Aumont, B.: Structure-activity relationships to estimate the effective Henry's law constants of organics of atmospheric interest, Atmospheric Chemistry and Physics, 10, 7643–7654, https://doi.org/10.5194/acp-10-7643-2010, 2010.

Rockel, B., Will, A., and Hense, A.: The Regional Climate Model COSMO-CLM (CCLM), Meteorologische Zeitschrift, pp. 347–348, https://doi.org/10.1127/0941-2948/2008/0309, 2008.

Roeckner, E., Brokopf, R., Esch, M., Giorgetta, M., Hagemann, S., Kornblueh, L., Manzini, E., Schlese, U., and Schulzweida, U.: Sensitivity of Simulated Climate to Horizontal and Vertical Resolution in the ECHAM5 Atmosphere Model, Journal of Climate, 19, 3771–3791, https://doi.org/10.1175/JCLI3824.1, 2006.

Rosanka, S., Sander, R., Wahner, A., and Taraborrelli, D.: Oxidation of low-molecular-weight organic compounds in cloud droplets: development of the Jülich Aqueous-phase Mechanism of Organic Chemistry (JAMOC) in CAABA/MECCA (version 4.5.0), Geoscientific Model Development, 14, 4103–4115, https://doi.org/10.5194/gmd-14-4103-2021, 2021.

Rosanka, S., Tost, H., Sander, R., Jöckel, P., Kerkweg, A., and Taraborrelli, D.: How non-equilibrium aerosol chemistry impacts particle acidity: the GMXe AERosol CHEMistry (GMXe–AERCHEM, v1.0) sub-submodel of MESSy, Geoscientific Model Development, 17, 2597–2615, https://doi.org/10.5194/gmd-17-2597-2024, 2024.

Sander, R.: Modeling Atmospheric Chemistry: Interactions between Gas-Phase Species and Liquid Cloud/Aerosol Particles, Surveys in Geophysics, 20, 1–31, https://doi.org/10.1023/A:1006501706704, 1999.

Sander, R., Baumgaertner, A., Gromov, S., Harder, H., Jöckel, P., Kerkweg, A., Kubistin, D., Regelin, E., Riede, H., Sandu, A., Taraborrelli, D., Tost, H., and Xie, Z.-Q.: The atmospheric chemistry box model CAABA/MECCA-3.0, Geoscientific Model Development, 4, 373–380, https://doi.org/10.5194/gmd-4-373-2011, 2011.

Sander, R., Baumgaertner, A., Cabrera-Perez, D., Frank, F., Gromov, S., Grooß, J.-U., Harder, H., Huijnen, V., Jöckel, P., Karydis, V. A., Niemeyer, K. E., Pozzer, A., Riede, H., Schultz, M. G., Taraborrelli, D., and Tauer, S.: The community atmospheric chemistry box model CAABA/MECCA-4.0, Geoscientific Model Development, 12, 1365–1385, https://doi.org/10.5194/gmd-12-1365-2019, 2019.

Schwartz, S. E.: Mass-Transport Considerations Pertinent to Aqueous Phase Reactions of Gases in Liquid-Water Clouds, in: Chemistry of Multiphase Atmospheric Systems, edited by Jaeschke, W., pp. 415–471, Springer, Berlin, Heidelberg, ISBN 978-3-642-70627-1, https://doi.org/10.1007/978-3-642-70627-1_16, 1986.

Sommariva, R., Cox, S., Martin, C., Borońska, K., Young, J., Jimack, P. K., Pilling, M. J., Matthaios, V. N., Nelson, B. S., Newland, M. J., Panagi, M., Bloss, W. J., Monks, P. S., and Rickard, A. R.: AtChem (version 1), an open-source box model for the Master Chemical Mechanism, Geoscientific Model Development, 13, 169–183, https://doi.org/10.5194/gmd-13-169-2020, 2020.

Stokes, R. H. and Robinson, R. A.: Interactions in Aqueous Nonelectrolyte Solutions. I. Solute-Solvent Equilibria, The Journal of Physical Chemistry, 70, 2126–2131, https://doi.org/10.1021/j100879a010, 1966.

Suda, S. R., Petters, M. D., Yeh, G. K., Strollo, C., Matsunaga, A., Faulhaber, A., Ziemann, P. J., Prenni, A. J., Carrico, C. M., Sullivan, R. C., and Kreidenweis, S. M.: Influence of Functional Groups on Organic Aerosol Cloud Condensation Nucleus Activity, Environmental Science & Technology, 48, 10 182–10 190, https://doi.org/10.1021/es502147y, 2014.

https://doi.org/10.5194/egusphere-2026-4522
Preprint. Discussion started: 13 August 2026

Taraborrelli, D., Lawrence, M. G., Crowley, J. N., Dillon, T. J., Gromov, S., Groß, C. B. M., Vereecken, L., and Lelieveld, J.: Hydroxyl radical buffered by isoprene oxidation over tropical forests, Nature Geoscience, 5, 190–193, https://doi.org/10.1038/ngeo1405, 2012.

Taraborrelli, D., Cabrera-Perez, D., Bacer, S., Gromov, S., Lelieveld, J., Sander, R., and Pozzer, A.: Influence of aromatics on tropospheric gas-phase composition, Atmospheric Chemistry and Physics, 21, 2615–2636, https://doi.org/10.5194/acp-21-2615-2021, 2021.

The MESSy Consortium, .: The Modular Earth Submodel System (Versions d2.55.2$_s$52$-$$kinetic_chamexp-2dev_6$878788$d$), $Zenodo$, , 2026.

Topping, D., Barley, M., Bane, M. K., Higham, N., Aumont, B., Dingle, N., and McFiggans, G.: UManSysProp v1.0: an online and open-source facility for molecular property prediction and atmospheric aerosol calculations, Geoscientific Model Development, 9, 899–914, https://doi.org/10.5194/gmd-9-899-2016, 2016.

Tost, H., Jöckel, P., Kerkweg, A., Sander, R., and Lelieveld, J.: Technical note: A new comprehensive SCAVenging submodel for global atmospheric chemistry modelling, Atmospheric Chemistry and Physics, 6, 565–574, https://doi.org/10.5194/acp-6-565-2006, 2006.

Varutbangkul, V., Brechtel, F. J., Bahreini, R., Ng, N. L., Keywood, M. D., Kroll, J. H., Flagan, R. C., Seinfeld, J. H., Lee, A., and Goldstein, A. H.: Hygroscopicity of secondary organic aerosols formed by oxidation of cycloalkenes, monoterpenes, sesquiterpenes, and related compounds, Atmospheric Chemistry and Physics, 6, 2367–2388, https://doi.org/10.5194/acp-6-2367-2006, 2006.

Wang, W., Lei, T., Zuend, A., Su, H., Cheng, Y., Shi, Y., Ge, M., and Liu, M.: Effect of mixing structure on the water uptake of mixtures of ammonium sulfate and phthalic acid particles, Atmospheric Chemistry and Physics, 21, 2179–2190, https://doi.org/10.5194/acp-21-2179-2021, 2021.

Weininger, D.: SMILES, a chemical language and information system. 1. Introduction to methodology and encoding rules, Journal of Chemical Information and Computer Sciences, 28, 31–36, https://doi.org/10.1021/ci00057a005, 1988.

Wieser, F., Sander, R., Cho, C., Fuchs, H., Hohaus, T., Novelli, A., Tillmann, R., and Taraborrelli, D.: Development of a multiphase chemical mechanism to improve secondary organic aerosol formation in CAABA/MECCA (version 4.7.0), Geoscientific Model Development, 17, 4311–4330, https://doi.org/10.5194/gmd-17-4311-2024, 2024.

Wolfe, G. M., Marvin, M. R., Roberts, S. J., Travis, K. R., and Liao, J.: The Framework for 0-D Atmospheric Modeling (F0AM) v3.1, Geoscientific Model Development, 9, 3309–3319, https://doi.org/10.5194/gmd-9-3309-2016, 2016.